The Air Pollution Model (TAPM) Version 1: Technical Description and Examples

Peter J. Hurley
CSIRO Atmospheric Research
Private Bag 1, Aspendale,
Vic 3195, Australia

Abstract

Air pollution predictions for environmental impact assessments usually use Gaussian plume/puff models driven by observationally-based meteorological inputs. An alternative approach is to use prognostic meteorological and air pollution models, which have many advantages over the Gaussian approach and are now becoming a viable tool for performing year-long simulations. Continuing rapid increases in computing power are bringing this approach within reach of a desktop PC. This report provides a comprehensive technical description of a newly developed prognostic model called The Air Pollution Model (TAPM), and provides two example simulations which illustrate model performance.

1 Introduction

Air pollution models that can be used to predict pollution concentrations for periods of up to a year, are generally semi-empirical/analytic approaches based on Gaussian plumes or puffs. These models typically use either a simple surface based meteorological file or a diagnostic wind field model based on available observations. The Air Pollution Model (TAPM) is different to these approaches in that it solves the fundamental fluid dynamics and scalar transport equations to predict meteorology and pollutant concentration for a range of pollutants important for air pollution applications. It consists of coupled prognostic meteorological and air pollution concentration components, eliminating the need to have site-specific meteorological observations. Instead, the model predicts the flows important to local-scale air pollution, such as sea breezes and terrain induced flows, against a background of larger-scale meteorology provided by synoptic analyses.

The meteorological component of TAPM is an incompressible, non-hydrostatic, primitive equation model with a terrain-following vertical coordinate for three-dimensional simulations. The model solves the momentum equations for horizontal wind components, the incompressible continuity equation for vertical velocity, and scalar equations for potential virtual temperature and specific humidity of water vapour, cloud water and rain water. The Exner pressure function is split into hydrostatic and non-hydrostatic components, and a Poisson equation is solved for the non-hydrostatic component. Explicit cloud micro-physical processes are included. The turbulence terms in these equations have been determined by solving equations for turbulence kinetic energy and eddy dissipation rate, and then using these values by representing the vertical fluxes by a gradient diffusion approach, including a counter-gradient term for heat flux. A vegetative canopy and soil scheme is used at the surface, while radiative fluxes, both at the surface and at upper levels, are also included.

The air pollution component of TAPM, which uses predicted meteorology and turbulence from the meteorological component, consists of three modules. The Eulerian Grid Module (EGM) solves prognostic equations for concentration and for cross-correlation of concentration and virtual potential temperature. The Lagrangian Particle Module (LPM) can be used to represent near-source dispersion more accurately, while the Plume Rise Module is used to account for plume momentum and buoyancy effects for point sources. The model also includes gas-phase photochemical reactions based on the Generic Reaction Set, and gas- and aqueous-phase chemical reactions for sulfur dioxide and particles. Wet and dry deposition effects are also included.

This report describes the technical details of the modelling approach in Section 2 and some example simulations in Section 3. The examples are for one month of meteorological predictions at the Cape Grim monitoring station in Tasmania, and for point source dispersion in the convective boundary layer, to illustrate the different results that can be expected from the EGM and LPM configurations of the model.

2 Meteorological component

The meteorological component of TAPM is an incompressible, non-hydrostatic, primitive equation model with a terrain-following vertical coordinate for three-dimensional simulations. It includes parameterisations for cloud micro-physical processes, turbulence closure, vegetative canopy and soil, and radiative fluxes.

In order to represent synoptic-scale meteorology in the model, we use an approach based on McNider and Pielke (1981), whereby pressure and temperature are written as a base-state plus synoptic and mesoscale perturbations. Under this approach, the synoptic-scale pressure gradient can be represented explicitly in the horizontal momentum equations as a function of the synoptic wind, which is provided to the model as an input. The pressure and temperature variables in the model represent the base-state plus the mesoscale perturbation, whereas the momentum equations are solved for the total wind components.

The model solution for horizontal wind components is weakly nudged towards the synoptic-scale input values of these variables. The virtual potential temperature and specific humidity predictions in all grid columns are nudged towards the synoptic profile at the centre of the domain. This is because these variables in the model only represent a base state plus mesoscale perturbation. Nudging towards the central synoptic-scale profile ensures that the base state is regularly updated.

The horizontal model domain size should be restricted in size to less than about 1000 km x 1000 km. The reasons for this restriction are that the model equations neglect the curvature of the earth and assume a constant coriolis force and a uniform distance grid spacing across the domain, and as described above, the synoptic scale perturbations to the pressure and temperature are neglected (except for their influence on the winds).

2.1 Base meteorological variables

The mean wind is determined for the horizontal components u and v (m s^{-1}) from the momentum equations and the terrain following vertical velocity $\dot{\sigma}$ (m s^{-1}) from the continuity equation. Potential virtual temperature θ_v (K) is determined from an equation combining conservation of heat and water vapour. The Exner pressure function $\pi = \pi_H + \pi_N$ (J kg^{-1} K^{-1})

is determined from the sum of the hydrostatic component π_H and non-hydrostatic component π_N (see Section 2.2). The equations for these variables are as follows

$$\frac{du}{dt} = F(u) + \frac{\partial \overline{w'u'}}{\partial \sigma}\frac{\partial \sigma}{\partial z} - \theta_v\left(\frac{\partial \pi}{\partial x} + \frac{\partial \pi}{\partial \sigma}\frac{\partial \sigma}{\partial x}\right) + f(v - v_s) - N_s(u - u_s) \quad (1)$$

$$\frac{dv}{dt} = F(v) + \frac{\partial \overline{w'v'}}{\partial \sigma}\frac{\partial \sigma}{\partial z} - \theta_v\left(\frac{\partial \pi}{\partial y} + \frac{\partial \pi}{\partial \sigma}\frac{\partial \sigma}{\partial y}\right) - f(u - u_s) - N_s(v - v_s) \quad (2)$$

$$\frac{\partial \dot{\sigma}}{\partial \sigma} = -\left(\frac{\partial u}{\partial x} + \frac{\partial v}{\partial y}\right) + u\frac{\partial}{\partial \sigma}\left(\frac{\partial \sigma}{\partial x}\right) + v\frac{\partial}{\partial \sigma}\left(\frac{\partial \sigma}{\partial y}\right) \quad (3)$$

$$\frac{d\theta_v}{dt} = F(\theta_v) + \frac{\partial \overline{w'\theta_v'}}{\partial \sigma}\frac{\partial \sigma}{\partial z} + S_{\theta_v} - N_s(\theta_v - \theta_{vs}) \quad (4)$$

$$\frac{\partial \pi_H}{\partial \sigma} = -\frac{g}{\theta_v}\left(\frac{\partial \sigma}{\partial z}\right)^{-1} \quad (5)$$

where

t = time (s),

x, y, σ = the terrain - following coordinates (m),

$\sigma = z_T\left(\frac{z - z_s}{z_T - z_s}\right)$,

z = cartesian vertical coordinate (m),

z_T = height of model top (m),

z_s = terrain height (m),

$\frac{d\phi}{dt} \equiv \frac{\partial \phi}{\partial t} + u\frac{\partial \phi}{\partial x} + v\frac{\partial \phi}{\partial y} + \dot{\sigma}\frac{\partial \phi}{\partial \sigma}$,

$F(\phi)$ = horizontal filtering of ϕ (see Section 4.3),

$\overline{w'\phi'}$ = vertical flux of ϕ (see Section 2.4),

f = Coriolis parameter $(4\pi_c \sin(lat)/(24 * 3600))$ (s^{-1}),

π_c = 3.14159265,

lat = latitude $(^o)$,

u_s, v_s, θ_{vs} = large scale synoptic winds and potential virtual temperature,

N_s = large scale nudging coefficient $(1/(2\Delta t_s))$,

Δt_s = time interval of synoptic analyses,

$S_{\theta_v} = \frac{\theta_v}{T}\left(\frac{\partial T}{\partial t}\right)_{RADIATION} - \frac{\lambda}{c_p}S_{q_V}$ (see Sections 2.3 and 2.5),

T = temperature (K),

g = gravitational constant $(9.81\ m\ s^{-2})$,

λ = latent heat of vaporisation of water $(2.5 \times 10^6\ J\ kg^{-1})$,

c_p = specific heat at constant pressure $(1006\ J\ kg^{-1}\ K^{-1})$,

$$\frac{\partial\sigma}{\partial x}=\left(\frac{\sigma-z_T}{z_T-z_s}\right)\frac{\partial z_s}{\partial x},\quad \frac{\partial\sigma}{\partial y}=\left(\frac{\sigma-z_T}{z_T-z_s}\right)\frac{\partial z_s}{\partial y},\quad \frac{\partial\sigma}{\partial z}=\left(\frac{z_T}{z_T-z_s}\right).$$

2.2 Non-hydrostatic pressure

The non-hydrostatic component of the Exner pressure function π_N is determined by taking spatial derivatives of the three momentum equations and the time derivative of the continuity equation, and then eliminating all time derivatives in the continuity equation by substitution. The following assumes all products of Coriolis terms and terrain gradients, and all turbulence and synoptic variation terms can be neglected. The resultant equation for π_N is

$$\begin{aligned}&\frac{\partial^2\pi_N}{\partial x^2}+2\frac{\partial\sigma}{\partial x}\frac{\partial^2\pi_N}{\partial x\partial\sigma}+\frac{\partial^2\pi_N}{\partial y^2}+2\frac{\partial\sigma}{\partial y}\frac{\partial^2\pi_N}{\partial y\partial\sigma}+\left(\frac{\partial\sigma}{\partial z}\right)^2\frac{\partial^2\pi_N}{\partial\sigma^2}\\&+C_x\frac{\partial\pi_N}{\partial x}+C_y\frac{\partial\pi_N}{\partial y}+C_\sigma\frac{\partial\pi_N}{\partial\sigma}=R_\pi,\end{aligned}\tag{6}$$

with coefficients

$$C_x=\frac{1}{\theta_v}\left(\frac{\partial\theta_v}{\partial x}+\frac{\partial\theta_v}{\partial\sigma}\frac{\partial\sigma}{\partial x}\right),\ C_y=\frac{1}{\theta_v}\left(\frac{\partial\theta_v}{\partial y}+\frac{\partial\theta_v}{\partial\sigma}\frac{\partial\sigma}{\partial y}\right),$$

$$C_\sigma=\frac{1}{\theta_v}\left(\frac{\partial\theta_v}{\partial x}\frac{\partial\sigma}{\partial x}+\frac{\partial\theta_v}{\partial y}\frac{\partial\sigma}{\partial y}+\frac{\partial\theta_v}{\partial\sigma}\left(\frac{\partial\sigma}{\partial z}\right)^2\right)+\frac{\partial^2\sigma}{\partial x^2}+\frac{\partial^2\sigma}{\partial y^2},$$

$$R_\pi=\frac{1}{\theta_v}\left(\frac{\partial R_u}{\partial x}+\frac{\partial R_v}{\partial y}+\frac{\partial R_{\dot\sigma}}{\partial\sigma}-R_u\frac{\partial}{\partial\sigma}\left(\frac{\partial\sigma}{\partial x}\right)-R_v\frac{\partial}{\partial\sigma}\left(\frac{\partial\sigma}{\partial y}\right)\right),$$

$$R_u=-u\frac{\partial u}{\partial x}-v\frac{\partial u}{\partial y}-\dot\sigma\frac{\partial u}{\partial\sigma}+f\left(v-v_g\right)-\theta_v\frac{\partial\pi_H}{\partial x}+g\frac{\partial\sigma}{\partial x}\left(\frac{\partial\sigma}{\partial z}\right)^{-1},$$

$$R_v=-u\frac{\partial v}{\partial x}-v\frac{\partial v}{\partial y}-\dot\sigma\frac{\partial v}{\partial\sigma}-f\left(u-u_g\right)-\theta_v\frac{\partial\pi_H}{\partial y}+g\frac{\partial\sigma}{\partial y}\left(\frac{\partial\sigma}{\partial z}\right)^{-1},$$

$$\begin{aligned}R_{\dot\sigma}=&-u\frac{\partial\dot\sigma}{\partial x}-v\frac{\partial\dot\sigma}{\partial y}-\dot\sigma\frac{\partial\dot\sigma}{\partial\sigma}-\theta_v\left(\frac{\partial\pi_H}{\partial x}\frac{\partial\sigma}{\partial x}+\frac{\partial\pi_H}{\partial y}\frac{\partial\sigma}{\partial y}\right)\\&+u^2\frac{\partial^2\sigma}{\partial x^2}+2uv\frac{\partial^2\sigma}{\partial x\partial y}+v^2\frac{\partial^2\sigma}{\partial y^2}+2\dot\sigma\left(u\frac{\partial}{\partial\sigma}\left(\frac{\partial\sigma}{\partial x}\right)+v\frac{\partial}{\partial\sigma}\left(\frac{\partial\sigma}{\partial y}\right)\right),\end{aligned}$$

and

$$\frac{\partial}{\partial\sigma}\left(\frac{\partial\sigma}{\partial x}\right)=\left(\frac{1}{z_T-z_s}\right)\frac{\partial z_s}{\partial x},\ \frac{\partial}{\partial\sigma}\left(\frac{\partial\sigma}{\partial y}\right)=\left(\frac{1}{z_T-z_s}\right)\frac{\partial z_s}{\partial y},$$

$$\frac{\partial^2\sigma}{\partial x^2}=\left(\frac{\sigma-z_T}{z_T-z_s}\right)\frac{\partial^2 z_s}{\partial x^2},\frac{\partial^2\sigma}{\partial x\partial y}=\left(\frac{\sigma-z_T}{z_T-z_s}\right)\frac{\partial^2 z_s}{\partial x\partial y},\frac{\partial^2\sigma}{\partial y^2}=\left(\frac{\sigma-z_T}{z_T-z_s}\right)\frac{\partial^2 z_s}{\partial y^2}.$$

2.3 Water and micro-physics

Conservation equations are solved for specific humidities (kg kg^{-1}) $q = q_V + q_C$ and q_R representing the sum of water vapour and cloud water, and rain water respectively

$$\frac{dq}{dt} = \frac{\partial \overline{u'q'}}{\partial x} + \frac{\partial \overline{v'q'}}{\partial y} + \frac{\partial \overline{w'q'}}{\partial \sigma}\frac{\partial \sigma}{\partial z} + S_{q_V} + S_{q_C} - N_s\left(q_V - q_{Vs}\right) \tag{7}$$

$$\frac{dq_R}{dt} = \frac{\partial \overline{u'q'_R}}{\partial x} + \frac{\partial \overline{v'q'_R}}{\partial y} + \frac{\partial \overline{w'q'_R}}{\partial \sigma}\frac{\partial \sigma}{\partial z} + S_{q_R} - \mathrm{V_T}\frac{\partial q_R}{\partial \sigma}\frac{\partial \sigma}{\partial z} \tag{8}$$

with

$S_{q_V}, S_{q_C}, S_{q_R}$ = micro– physical source terms,

q_{Vs} = synoptic scale specific humidity of water vapour,

V_T = rainfall terminal velocity,

and the specific humidity of water vapour q_V and the saturated specific humidity q_S determined from

$q_V = \min(q, q_S)$,

$$q_S = \frac{0.622 e_S}{(p - 0.378 e_S)},$$

p = pressure (Pa), and

$$e_S = 6.1 \exp\left(\frac{\lambda}{R_v}\left(\frac{1}{273.15} - \frac{1}{T}\right)\right).$$

Micro-physics is based on Katzfey and Ryan (1997) for warm rain (ice processes are generally important only for temperatures less than -10 °C), and includes bulk parameterisations for condensation of water vapor, evaporation of cloud water and rain water, auto-conversion and collection of cloud water to form rain water, and an expression for the rainfall terminal velocity.

The source terms in the water conservation equations are determined by

$$S_{q_V} = -P_{VC} - P_{VR}, \quad S_{q_C} = P_{VC} - P_{CR}, \quad S_{q_R} = P_{CR} + P_{VR},$$

where

$$P_{VC} = \left(\frac{q_V - q_S}{\Delta t}\right)\left(1 + \frac{\lambda}{c_p}\frac{dq_S}{dT}\right)^{-1}$$

$$P_{CR} = 0.057 g \max\left(0, q_C - 0.0001\right)\left(\frac{\rho^4 q_C^7}{N_C \rho_W}\right)^{1/3} + 0.884 q_C q_R \left(\frac{g \lambda_R \rho}{\rho_W}\right)^{1/2}$$

$$P_{VR} = \min\left(0, \frac{q_V}{q_{VS}} - 1\right)\frac{q_R \lambda_R^2}{\rho_W}\left(\frac{0.5 + \frac{0.349}{\mu^{1/2}}\left(\frac{\rho_W g \rho}{\lambda_R^3}\right)^{1/4}}{\frac{\lambda^2}{K R_V T^2} + \frac{R_V T}{e_{VS} D_V}}\right).$$

The rainfall terminal velocity is determined from : $V_T = -2.13\left(\frac{2g\rho_W}{\lambda_R \rho}\right)^{1/2}$.

Constants are

$N_C = 5\times10^7$ m^{-3}, $\lambda_R = 3846$ m^{-1}, $\rho_W = 1000$ kg m^{-3}, $R_V = 461.5$ J kg^{-1} K^{-1},
$\mu = 1.8\times10^{-5}$ kg m^{-1} s, $K = 0.025$ J m^{-1} s^{-1}, $D_V = 2.5\times10^{-5}$ m^2 s^{-1}.

Calculation of the precipitation rate (m s^{-1}) at the surface is from $P = \frac{\rho}{\rho_W} V_T q_R(0)$, where $q_R(0)$ is the amount of rain reaching the ground.

2.4 Turbulence and diffusion

Turbulence closure in the mean equations uses a gradient diffusion approach which depends on a diffusion coefficient *K* and gradients of mean variables, and includes a counter-gradient correction for potential virtual temperature based on Deardorff (1966). Using Cartesian tensor notation, the fluxes are

$$\overline{u_i' u_j'} = \frac{2}{3} E \delta_{ij} - K\left(\frac{\partial u_i}{\partial x_j} + \frac{\partial u_j}{\partial x_i}\right),$$

$$\overline{u_i' \phi'} = -K\left(\frac{\partial \phi}{\partial x_i} - \gamma_\phi\right),$$

where

i, j are subscripts for the three coordinate directions (i.e. $i = 1,2,3$ for *x,y,z* respectively),

u_i, u_j represent velocities,

$\delta_{ij} = \begin{cases} 1 \text{ if } i = j, \\ 0 \text{ otherwise.} \end{cases}$

ϕ represents a scalar,

γ_ϕ is zero, except for the vertical flux of θ_v ($\gamma_{\theta_v} = 0.00065$ K m^{-1}).

The turbulence scheme used to calculate *K* is the standard *E*-ε model in 3-d terrain-following coordinates, with constants for the eddy dissipation rate equation derived from the analysis of Duynkerke (1988). The model solves prognostic equations for the turbulence kinetic energy (*E*) and the eddy dissipation rate (ε)

$$\frac{dE}{dt} = \frac{\partial}{\partial x}\left(K\frac{\partial E}{\partial x}\right) + \frac{\partial}{\partial y}\left(K\frac{\partial E}{\partial y}\right) + \left(\frac{\partial \sigma}{\partial z}\right)^2 \frac{\partial}{\partial \sigma}\left(K\frac{\partial E}{\partial \sigma}\right) + P_s + P_b - \varepsilon, \tag{9}$$

$$\frac{d\varepsilon}{dt} = \frac{\partial}{\partial x}\left(K\frac{\partial \varepsilon}{\partial x}\right) + \frac{\partial}{\partial y}\left(K\frac{\partial \varepsilon}{\partial y}\right) + \left(\frac{\partial \sigma}{\partial z}\right)^2 \frac{\partial}{\partial \sigma}\left(c_{\varepsilon 0} K\frac{\partial \varepsilon}{\partial \sigma}\right)$$
$$+ \frac{\varepsilon}{E}(c_{\varepsilon 1} \max(P_s, P_s + P_b) - c_{\varepsilon 2}\varepsilon), \tag{10}$$

where

$$P_s = 2K\left(\left(\frac{\partial u}{\partial x}+\frac{\partial u}{\partial \sigma}\frac{\partial \sigma}{\partial x}\right)^2+\left(\frac{\partial v}{\partial y}+\frac{\partial v}{\partial \sigma}\frac{\partial \sigma}{\partial y}\right)^2+\left(\frac{\partial w}{\partial \sigma}\frac{\partial \sigma}{\partial z}\right)^2\right)$$
$$+K\left(\left(\frac{\partial u}{\partial y}+\frac{\partial u}{\partial \sigma}\frac{\partial \sigma}{\partial y}+\frac{\partial v}{\partial x}+\frac{\partial v}{\partial \sigma}\frac{\partial \sigma}{\partial x}\right)^2\right)$$
$$+K\left(\left(\frac{\partial u}{\partial \sigma}\frac{\partial \sigma}{\partial z}+\frac{\partial w}{\partial x}+\frac{\partial w}{\partial \sigma}\frac{\partial \sigma}{\partial x}\right)^2+\left(\frac{\partial v}{\partial \sigma}\frac{\partial \sigma}{\partial z}+\frac{\partial w}{\partial y}+\frac{\partial w}{\partial \sigma}\frac{\partial \sigma}{\partial y}\right)^2\right),$$

$$P_b = -\frac{g}{\theta_v}K\left(\frac{\partial \theta_v}{\partial \sigma}\frac{\partial \sigma}{\partial z}-\gamma_{\theta_v}\right),$$

with $w=\left(\frac{\partial \sigma}{\partial z}\right)^{-1}\left(\dot{\sigma}-u\frac{\partial \sigma}{\partial x}-v\frac{\partial \sigma}{\partial y}\right)$,

and $K = c_m\frac{E^2}{\varepsilon}$, $c_m = 0.09$, $c_{\varepsilon 0} = 0.69$, $c_{\varepsilon 1} = 1.46$, and $c_{\varepsilon 2} = 1.83$.

As an alternative to Equation (10) the model has an option to use a diagnostic eddy dissipation rate based on Duynkerke and Driedonks (1987). In this approach,

$$\varepsilon = c_m^{3/4}\frac{E^{3/2}}{l},$$
$$l = \min(l_b, l_s),$$
$$l_b = \left(\frac{\phi_M}{kz}+\frac{1}{l_o}\right)^{-1},$$
$$l_s = 0.36E^{1/2}\left(\frac{g}{\theta_v}\frac{\partial \theta_v}{\partial z}\right)^{-1/2},$$
$$l_o = 0.3\frac{\int Ezdz}{\int Edz},$$

ϕ_M = Surface layer similarity function (see Section 2.6.3),

k = von Karman constant (0.4).

2.5 Radiation

2.5.1 Clear-sky

Radiation at the surface is used for the computation of surface boundary conditions and scaling variables (see later), with the clear-sky incoming shortwave component from Mahrer and Pielke (1977),

$$R^{in}_{sw(clear-sky)} = \begin{cases}(a_g - a_w(z_s))S_{\text{Slope}}S_o\cos\chi; & \text{for } \cos\chi > 0\\ 0; & \text{for } \cos\chi \le 0\end{cases},$$

and the clear-sky incoming long-wave component from Dilley and O'Brien (1999),

$$R^{in}_{lw(clear-sky)} = \left(59.38 + 113.7\left(\frac{T(\sigma_1)}{273.15}\right)^6 + 96.96\left(\frac{r(\sigma_1)}{25}\right)^{1/2}\right)\cos\alpha,$$

with

$$a_g = 0.485 + 0.515\left(1.014 - 0.16/\sqrt{\cos\chi}\right),$$

$$a_w(\sigma) = 0.039\left(\frac{r(\sigma)}{\cos\chi}\right)^{0.3},$$

$r(\sigma) = \int_{\sigma}^{z_T} \rho q d\sigma$ is the column water vapour amount (kg m^{-2} or mm) between z_T and σ,

χ is the zenith angle, and S_o is the solar constant (1367 W m^{-2}).

The solar declination, zenith, and terrain slope angles are calculated using

$$\sin\delta_s = \sin(23.5\pi_c/180)\sin(2\pi_c\, day/365),$$

$$\cos\chi = \cos(lat)\cos\delta_s\cos(\pi_c(hour-12)/12) + \sin(lat)\sin\delta_s,$$

$$S_{\text{Slope}} = \frac{\cos i}{\cos\chi}, \quad \cos i = \cos\alpha\cos\chi + \sin\alpha\sin\chi\cos(\beta-\eta),$$

$$\alpha = \tan^{-1}\left(\left(\frac{\partial z_s}{\partial x}\right)^2 + \left(\frac{\partial z_s}{\partial y}\right)^2\right), \quad \eta = \tan^{-1}\left(\left(\frac{\partial z_s}{\partial y}\right)\left(\frac{\partial z_s}{\partial x}\right)^{-1}\right) - \frac{\pi_c}{2},$$

$$\beta = \sin^{-1}(\cos\delta_s\sin(\pi_c(hour-12)/12)/\sin\chi),$$

lat = latitude, day = day of year ($1 \equiv 21$ March),

$hour$ = hour of day (24 hour clock), $\pi_c = 3.14159265$.

2.5.2 Cloudy sky

The clear-sky incoming radiation components from the previous section are modified for liquid water effects using an approach based on Stephens (1978). The method ignores any heating/cooling effects of water vapour and other gases in non-cloudy layers, and assumes clear and cloudy sky contributions can be treated separately.

Incoming shortwave radiation at the model top is initialised with the value

$$R^{in}_{sw}(z_T) = R^{in}_{sw(clear-sky)},$$

and this value is modified by integrating downwards for each model level and to the surface using

$$R^{in}_{sw}(\sigma) = R^{in}_{sw}(\sigma + \Delta\sigma)\Psi_{Transmission},$$

and using a fit to within 0.05 of the Ψ functions from Figure 3 of Stephens (1978) for the transmission/absorption of shortwave radiation (ignoring zenith angle dependence)

$$\Psi_{Transmission} = \begin{cases} \exp(-16W + 13W^2); & W \le 0.25 \\ 0.04; & W > 0.25 \end{cases},$$

$$\Psi_{Absorption} = \begin{cases} 0.3W; & W \le 0.25 \\ 0.15; & W > 0.25 \end{cases}.$$

Incoming longwave radiation at the model top is initialised with the value

$$R_{lw}^{in}(z_T) = R_{lw(clear-sky)}^{in},$$

and this value is modified by integrating downwards for each model level and to the surface using

$$R_{lw}^{in}(\sigma) = R_{lw}^{in}(\sigma + \Delta\sigma)\left(1 - \varepsilon_{lw}^{in}(\sigma)\right) + \varepsilon_{lw}^{in}(\sigma)\sigma_{SB}T^4(\sigma),$$
$$\varepsilon_{lw}^{in}(\sigma) = 1 - \exp(-158W), \text{ and}$$
$$W = \rho(q_C + q_R)\Delta\sigma.$$

Radiative heating and cooling at each model level is accounted for via the source term in the prognostic equation for temperature with

$$\left.\frac{\partial T}{\partial t}\right|_{RADIATION} = \frac{1}{\rho c_p}\frac{\partial \Psi_{Heat}}{\partial \sigma}\frac{\partial \sigma}{\partial z},$$

where for each model level

$$\Psi_{Heat}(\sigma) = R_{sw}^{in}(\sigma + \Delta\sigma)\Psi_{Absorption} + R_{lw}^{in}(\sigma) - R_{lw}^{out}(\sigma),$$

with the incoming shortwave and longwave components from the above expressions. The outgoing longwave radiation is calculated by initialising at the surface with

$$R_{lw}^{out}(z_s) = R_{lw(clear-sky)}^{out} = \sigma_{SB}T^4(z_s)\cos(\alpha),$$

and then modifying this value by integrating upwards for each model level using

$$R_{lw}^{out}(\sigma) = R_{lw}^{out}(\sigma - \Delta\sigma)\left(1 - \varepsilon_{lw}^{out}(\sigma)\right) + \varepsilon_{lw}^{out}(\sigma)\sigma_{SB}T^4(\sigma),$$
$$\varepsilon_{lw}^{out}(\sigma) = 1 - \exp(-130W),$$
$$W = \rho(q_C + q_R)\Delta\sigma,$$

where $\sigma_{SB} = 5.67 \times 10^8$ W m^{-2} K^{-4} is the Stefan Boltzman constant.

2.6 Surface boundary conditions

Boundary conditions for mean variables at the surface are zero velocity, π_0 from the hydrostatic equation (5), $\theta_{v0} = c_p T_0(1 + 0.61q_0)/\pi_0$, with $T_0 = (1-\sigma_f)T_g + \sigma_f T_f$ and $q_0 = (1-\sigma_f)q_g + \sigma_f q_f$, where σ_f is the fraction of foliage cover and subscripts g and f denote soil and foliage respectively. The soil and vegetation parameterisations described below are based on those from Kowalczyk *et al.* (1991).

2.6.1 Soil parameterisation

Equations for soil temperature T_g, moisture content η_g and specific humidity q_g are

$$\frac{\partial \mathrm{T}_g}{\partial \mathrm{t}} = \frac{3.72G_g}{\rho_s c_s d_1'} - \frac{7.4(T_g - T_d)}{24 \times 3600},$$

$$\frac{\partial \eta_g}{\partial \mathrm{t}} = -\frac{c_1\left(E_g(1-\sigma_f) - \rho_w\left((1-\sigma_f)P + \sigma_f P_g\right)\right)}{\rho_w d_1} - \frac{c_2(\eta_g - \eta_{eq})}{24\times 3600},$$

$$q_g = f_{wet} q_0^* + (1 - f_{wet}) q_1,$$

where

$G_g = R_{sw}^{in}(1-\alpha_g) + R_{lw}^{in} - \sigma_{SB} T_g^4 \cos\alpha - H_g - \lambda E_g =$ soil heat flux (W m^{-2}),

$H_g = \rho c_p(\theta_g - \theta_1)/r_H =$ sensible heat flux (W m^{-2}),

$\lambda E_g = \rho\lambda(q_g - q_1)/r_H =$ evaporative heat flux (W m^{-2}),

r_{H} is the aerodynamic resistance (see Section 2.6.3),

$$\eta_{\mathrm{eq}} = \eta_{\mathrm{d}} - \eta_{\mathrm{sat}} a_\eta \left(\frac{\eta_{\mathrm{d}}}{\eta_{\mathrm{sat}}}\right)^{b_\eta}\left(1 - \left(\frac{\eta_{\mathrm{d}}}{\eta_{\mathrm{sat}}}\right)^{8b_\eta}\right),$$

$T_d, \eta_d =$ deep soil temperature and moisture (model input),

$\lambda = 2.5\times 10^6$ J kg^{-1}, $\rho_w = 1000$ kg m^{-3},

$$d_1' = \sqrt{\frac{k_s \times 24\times 3600}{\rho_s c_s \pi_c}},\ d_1 = 0.1,$$

$\alpha_{\mathrm{g}}, k_s, \rho_s, c_s =$ soil albedo, conductivity, density, and heat capacity,

$P, P_g =$ precipitation reaching the vegetation and soil respectively,

$q_g^* =$ soil saturated specific humidity.

The soil characteristics are specified for three soil types

$k_s = 419(a_s\eta_g - b_s\eta_g^{0.4}),$

$\rho_s c_s = (1-\eta_{sat})\rho_s^{dry} c_s^{dry} + \eta_g \rho_w c_w,$

$c_w = 4186,$

Sand:

$$c_1 = \begin{cases} 10 & ;\ \text{for } \eta_r \le 0.05, \\ \dfrac{(1.8\eta_r + 0.962)}{(5.0\eta_r + 0.2)} & ;\ \text{otherwise.} \end{cases}$$

$c_2 = 2.0;$

$$f_{wet} = \begin{cases} 1 & ;\ \text{for } \eta_r \ge 0.15, \\ 11.49(\eta_r - 0.063) & ;\ \text{for } 0.063 \le \eta_r \le 0.15, \\ 0 & ;\ \text{for } \eta_r < 0.063. \end{cases}$$

$\eta_r = \eta_0 / \eta_{sat}, \eta_{sat} = 0.395, \eta_{wilt} = 0.068,$

$a_s = 0.004, b_s = 0.006, \rho_s^{dry} = 1600, c_s^{dry} = 800, a_\eta = 0.387, b_\eta = 4.$

Sandy Clay Loam:

$$c_1 = \begin{cases} 10 & ;\ \text{for } \eta_r \le 0.226, \\ \dfrac{(1.78\eta_r + 0.253)}{(2.96\eta_r - 0.581)} & ;\ \text{otherwise.} \end{cases}$$

$$c_2 = 3.0;$$

$$f_{wet} = \begin{cases} 1 & ;\ \text{for } \eta_r \ge 0.365, \\ 6.90(\eta_r - 0.22) & ;\ \text{for } 0.22 \le \eta_r \le 0.365, \\ 0 & ;\ \text{for } \eta_r < 0.22. \end{cases}$$

$$\eta_r = \eta_0 / \eta_{sat}, \eta_{sat} = 0.420, \eta_{wilt} = 0.175,$$

$$a_s = 0.003, b_s = 0.004, \rho_s^{dry} = 1600, c_s^{dry} = 845, a_\eta = 0.135, b_\eta = 6.$$

Clay:

$$c_1 = \begin{cases} 10 & ;\ \text{for } \eta_r \le 0.421, \\ \dfrac{(2.22\eta_r - 0.556)}{(2.78\eta_r - 1.114)} & ;\ \text{otherwise.} \end{cases}$$

$$c_2 = 1.9;$$

$$f_{wet} = \begin{cases} 1 & ;\ \text{for } \eta_r \ge 0.52, \\ 8.33(\eta_r - 0.40) & ;\ \text{for } 0.40 \le \eta_r \le 0.52, \\ 0 & ;\ \text{for } \eta_r < 0.40. \end{cases}$$

$$\eta_r = \eta_0 / \eta_{sat}, \eta_{sat} = 0.482, \eta_{wilt} = 0.286,$$

$$a_s = 0.002, b_s = 0.003, \rho_s^{dry} = 1600, c_s^{dry} = 890, a_\eta = 0.083, b_\eta = 12.$$

2.6.2 Vegetation parameterisation

The vegetation temperature T_f is calculated from a surface energy balance

$$0 = R_{sw}^{in}(1-\alpha_f) + R_{lw}^{in} - \sigma_{SB} T_f^4 \cos\alpha - H_f - \lambda E_f$$

using Newton iteration, where the outward long wave radiation and sensible (H_f) and latent (E_f) heat fluxes are treated as functions of T_f, with

$$H_f = \rho c_p(\theta_f - \theta_1)/r_H,$$

$$E_f = (1-\beta)E_{tr} + \beta E_w,$$

$$E_{tr} = \rho(q_f^* - q_1)/(r_H + r_s),$$

$$E_w = \rho(q_f^* - q_1)/r_H,$$

$$\beta = \begin{cases} 1; & \text{if condensation } (q_1 > q_f^*) \\ m_r/(0.0002LAI); & \text{if evapotranspiration} \end{cases},$$

$$\frac{\partial m_r}{\partial t} = P - \beta E_w / \rho_w,$$

where m_r is the moisture reservoir and r_H is the aerodynamic resistance (see Section 2.6.3).

Table 1: Vegetation (land-use) characteristics used in TAPM.

Vegetation Types:	h_f (m)	σ_f	LAI	r_{si} (m^{-1})
1: Forest – tall dense	42.00	0.75	4.8	370
2: Forest – tall mid-dense	36.50	0.75	6.3	330
3: Forest – dense	25.00	0.75	5.0	260
4: Forest - mid-dense	17.00	0.50	3.8	200
5: Forest - sparse (woodland)	12.00	0.25	2.8	150
6: Forest - very sparse (woodland)	10.00	0.25	2.5	130
7: Forest - low dense	9.00	0.75	3.9	200
8: Forest - low mid-dense	7.00	0.50	2.8	150
9: Forest - low sparse (woodland)	5.50	0.25	2.0	110
10: Shrubland - tall mid-dense (scrub)	3.00	0.50	2.6	160
11: Shrubland - tall sparse	2.50	0.25	1.7	100
12: Shrubland - tall very sparse	2.00	0.25	1.9	120
13: Shrubland - low mid-dense	1.00	0.50	1.4	90
14: Shrubland - low sparse	0.60	0.25	1.5	90
15: Shrubland - low very sparse	0.50	0.25	1.2	80
16: Grassland – sparse hummock	0.50	0.25	1.6	90
17: Grassland - very sparse hummock	0.45	0.25	1.4	90
18: Grassland – dense tussock	0.75	0.75	2.3	150
19: Grassland - mid-dense tussock	0.60	0.50	1.2	80
20: Grassland – sparse tussock	0.45	0.25	1.7	100
21: Grassland - very sparse tussock	0.40	0.25	1.2	80
22: Pasture/herbfield - dense (perennial)	0.60	0.75	2.3	80
23: Pasture/herbfield - dense (seasonal)	0.60	0.75	2.3	80
24: Pasture/herbfield - mid-dense (perennial)	0.45	0.50	1.2	40
25: Pasture/herbfield - mid-dense (seasonal)	0.45	0.50	1.2	40
26: Pasture/herbfield – sparse	0.35	0.25	1.9	120
27: Pasture/herbfield – very sparse	0.30	0.25	1.0	80
28: Littoral	2.50	0.50	3.0	180
29: Permanent lake	0.00	0.00	2.0	100
30: Ephemeral lake (salt)	0.00	0.00	2.0	100
31: Urban	10.00	0.75	2.0	100

The vegetation specific humidity q_f is calculated from $q_f = q_f^* - E_f r_S / \rho$, and the stomatal resistance r_S is calculated using

$$r_S = \frac{r_{si}}{LAI} F_1 F_2^{-1} F_3^{-1} F_4^{-1}$$

and

$$F_1 = \frac{1+f}{f + (r_{si}/5000)}, \quad F_2 = \frac{\eta_d - \eta_{wilt}}{0.75\eta_{sat} - \eta_{wilt}},$$

$$F_3 = 1 - 0.00025(e_f^* - e_1), \quad F_4 = 1 - 0.0016(298 - T_1)^2, \quad f = 0.55 \frac{\mathrm{R}_{\mathrm{sw}}^{\mathrm{in}}}{\mathrm{R}^*} \frac{2}{LAI}.$$

Other variables are

α_f = Vegetation albedo (0.2),

q_f^* = Vegetation saturated specific humidity,

e_f^* = Vegetation saturated vapour pressure,

$$R^* = \begin{cases} 30 \text{ W m}^{-2}; & \text{if } z_{0f} > 0.3 \\ 100 \text{ W m}^{-2}; & \text{if } z_{0f} \le 0.3 \end{cases},$$

z_{0f} = Vegetation roughness length (m) = $h_f / 10$ $(0.05 \le z_{0f} \le 1.00)$,

h_f = Vegetation height (m),

σ_f = Fraction of surface covered by vegetation,

LAI = Leaf Area Index,

r_{si} = minimum stomatal resistance (s^{-1}).

The vegetation (land-use) types used in TAPM are based on a CSIRO Wildlife and Ecology Categorisation (Graetz, 1998, personal communication), and are listed in Table 1.

2.6.3 Surface fluxes and turbulence

Boundary conditions for the turbulent fluxes are determined by Monin-Obukhov surface layer scaling variables with stability functions from Dyer and Hicks (1970)

$$\overline{w'u'}\big|_0 = -u_*^2 u \Big/ \sqrt{u_1^2 + v_1^2}, \quad \overline{w'v'}\big|_0 = -u_*^2 v \Big/ \sqrt{u_1^2 + v_1^2}, \quad \overline{w'\theta_v'}\big|_0 = -u_* \theta_{v*}, \quad \overline{w'q'}\big|_0 = -u_* q_*.$$

where

$$u_* = k\sqrt{u_1^2 + v_1^2} / I_M, \theta_{v*} = k(\theta_{v1} - \theta_{v0}) / I_H, \theta_* = k(\theta_1 - \theta_0) / I_H, q_* = k(q_1 - q_0) / I_H,$$

$$I_M = \begin{cases} \ln\left(\frac{z_1}{z_0}\right) - 2\ln\left(\frac{1 + \phi_M^{-1}(z_1)}{1 + \phi_M^{-1}(z_0)}\right) - \ln\left(\frac{1 + \phi_M^{-2}(z_1)}{1 + \phi_M^{-2}(z_0)}\right) \\ \qquad + 2\left(\tan^{-1}\left(\phi_M^{-1}(z_1)\right) - \tan^{-1}\left(\phi_M^{-1}(z_0)\right)\right), \text{if } \frac{z_1}{L} < 0, \\ \ln\left(\frac{z_1}{z_0}\right) + 5\left(\frac{z_1 - z_0}{L}\right), \text{if } \frac{z_1}{L} \ge 0 \end{cases}$$

$$I_H = I_{aH} + I_{bH},$$

$$I_{aH} = \begin{cases} \ln\left(\frac{z_1}{z_0}\right) - 2\ln\left(\frac{1 + \phi_H^{-1}(z_1)}{1 + \phi_H^{-1}(z_T)}\right), \text{if } \frac{z_1}{L} < 0 \\ \ln\left(\frac{z_1}{z_0}\right) + 5\left(\frac{z_1 - z_T}{L}\right), \text{if } \frac{z_1}{L} \ge 0 \end{cases},$$

$$I_{bH} = \ln\left(\frac{z_0}{z_T}\right),$$

$r_H = I_H/(ku_*),\ r_{aH} = I_{aH}/(ku_*),\ r_{bH} = I_{bH}/(ku_*),$

$$\phi_M = \begin{cases} \left(1-16\frac{z}{L}\right)^{-1/4}; & \text{for } \frac{z}{L} < 0 \\ \left(1+5\frac{z}{L}\right); & \text{for } \frac{z}{L} \geq 0 \end{cases},\ \phi_H = \begin{cases} \left(1-16\frac{z}{L}\right)^{-1/2}; & \text{for } \frac{z}{L} < 0 \\ \left(1+5\frac{z}{L}\right); & \text{for } \frac{z}{L} \geq 0 \end{cases},$$

with $\frac{z}{L} = \frac{kzg\theta_{v*}}{u_*^2\theta_v}$, and $z_T = z_0/7.4$ from Garratt (1992),

and the gradient Richardson number $R_{ig} = \frac{z}{L}\frac{\phi_H}{\phi_M^2}$,

which in the stable limit gives a critical value of $R_{igc} = 0.2$.

These equations are solved iteratively, with the restrictions that $\sqrt{u_1^2 + v_1^2} \geq 0.5$ m s^{-1}, $z_1 / L \leq 1$, and $0.05 \leq u_* \leq 1.0$ m s^{-1}.

Turbulence boundary conditions are specified at the first model level using surface and mixed layer scaling, for the prognostic turbulence equations

$$E = c_m^{-1/2}u_*^2 + 0.5w_*^2 \text{ and } \varepsilon = \frac{u_*^3}{kz}\phi_m - \frac{g}{\theta_v}u_*\theta_{v*},$$

where w_* is the convective velocity scale (m s^{-1}) defined as

$$w_* = \left(\frac{-gz_i u_*\theta_{v*}}{\theta_v}\right)^{1/3},$$

and z_i is the convective boundary layer height (m). The boundary layer height in convective conditions is defined as the first model level above the surface for which the vertical heat flux is negative, while in stable/neutral conditions it is defined as the first model level above the surface that has a vertical heat flux less than 5% of the surface value following Derbyshire (1990).

2.7 Initial conditions and boundary conditions

The model is initialised at each grid point with values of $u_s, v_s, \theta_{vs}, q_s$ interpolated from the synoptic analyses. Iso-lines of these variables are oriented to be parallel to mean sea level (ie: cutting into the terrain). Turbulence levels are set to their minimum values as the model is started at midnight. The Exner pressure function is integrated from mean sea level to the model top to determine the top boundary condition. The Exner pressure and terrain-following vertical velocity are then diagnosed using equations (3) and (5) respectively. Surface temperature and moisture are set to the deep soil values specified, with surface temperature adjusted for terrain height using the synoptic lapse rate.

At the model top boundary, all variables are set at their synoptic values $u_s, v_s, \theta_{vs}, q_s$, while zero gradient boundary conditions are used for all variables at the lateral boundaries. The terrain is smoothed near the lateral boundaries to reduce noise created by the boundary conditions. If the nesting option is used, one-way nested boundary conditions are used for the prognostic equations (1), (2), (4), and (7) using an approach based on Davies (1976). For example for *u*, an additional term is added to the right hand side of equation (1).

$$\frac{du}{dt} = RHS(u) - F_{NEST}\,\frac{(u-\tilde{u})}{\Delta t}$$

where $\tilde{u}$ is interpolated from the coarse outer grid onto the fine inner grid, and

$$F_{NEST} = \max(G_x, G_y)$$

$$G_x = \begin{cases} 1-\left(\dfrac{i-1}{n_b}\right)^2; & \text{for } i = 1,...,n_b; \\ 1-\left(\dfrac{n_x - i}{n_b}\right)^2; & \text{for } i = n_x-(n_b-1),...,n_x; \\ 0; & \text{otherwise.} \end{cases}$$

and similarly for G_y, with n_x the number of grid points in the x direction, and $n_b = 5$ the number of grid points in from the grid edge over which the solutions are meshed.

3 Air pollution component

3.1 Eulerian grid module

The Eulerian Grid Module (EGM) consists of nestable grid-based solutions of the Eulerian concentration equation representing advection, diffusion, and chemical reactions. Dry and wet deposition processes are also included.

3.1.1 Pollutant equations

The prognostic equation for concentration χ is similar to that for the potential virtual temperature and specific humidity variables, and includes advection, diffusion, and terms to represent pollutant emissions S_χ and chemical reactions R_χ

$$\frac{d\chi}{dt} = \frac{\partial}{\partial x}\left(K_\chi \frac{\partial \chi}{\partial x}\right) + \frac{\partial}{\partial y}\left(K_\chi \frac{\partial \chi}{\partial y}\right) - \left(\frac{\partial \sigma}{\partial z}\right)\frac{\partial}{\partial \sigma}\left(\overline{w'\chi'}\right) + S_\chi + R_\chi. \tag{11}$$

The expression for the vertical flux of tracer concentration includes counter-gradient fluxes as follows

$$\overline{w'\chi'} = -K_\chi \frac{\partial \chi}{\partial \sigma}\frac{\partial \sigma}{\partial z} + \frac{(1-c_{\chi 3})}{c_{\chi 1}}\frac{E}{\varepsilon}\frac{g}{\theta_v}\overline{\theta_v'\chi'}$$

with

$$\begin{aligned} \frac{d\overline{\theta_v'\chi'}}{dt} = {} & \frac{\partial}{\partial x}\left(K_\chi \frac{\partial \overline{\theta_v'\chi'}}{\partial x}\right) + \frac{\partial}{\partial y}\left(K_\chi \frac{\partial \overline{\theta_v'\chi'}}{\partial y}\right) + \left(\frac{\partial \sigma}{\partial z}\right)^2 \frac{\partial}{\partial \sigma}\left(K_\chi \frac{\partial \overline{\theta_v'\chi'}}{\partial \sigma}\right) \\ & + \left(K + K_\chi\right)\left(\left(\frac{\partial \theta_v}{\partial x} + \frac{\partial \theta_v}{\partial \sigma}\frac{\partial \sigma}{\partial x}\right)\left(\frac{\partial \chi}{\partial x} + \frac{\partial \chi}{\partial \sigma}\frac{\partial \sigma}{\partial x}\right) + \left(\frac{\partial \theta_v}{\partial y} + \frac{\partial \theta_v}{\partial \sigma}\frac{\partial \sigma}{\partial y}\right)\left(\frac{\partial \chi}{\partial y} + \frac{\partial \chi}{\partial \sigma}\frac{\partial \sigma}{\partial y}\right)\right) \\ & - \overline{w'\theta_v'}\frac{\partial \chi}{\partial \sigma}\frac{\partial \sigma}{\partial z} - \overline{w'\chi'}\frac{\partial \theta_v}{\partial \sigma}\frac{\partial \sigma}{\partial z} - \frac{2}{c_\chi}\frac{\varepsilon}{E}\overline{\theta_v'\chi'}. \end{aligned} \tag{12}$$

Constants in these equations are $c_{\chi 1} = 3.0, c_{\chi 3} = 0.5,$ and $c_{\chi} = 1.6,$ based on those used by Rodi (1985). The form of these equations has been used in many of the second order closure models for a meteorological scalar, and has been used by Enger (1986) for dispersion in a convective boundary layer, although he also used a prognostic equation for $\overline{w'\chi'}$. The diffusion coefficient used for pollutant concentration is $K_{\chi} = 2.5K$, where K is the diffusion coefficient for meteorological variables (see section 2.4), and the coefficient of 2.5 is based on an analysis of the second order closure equations from Andren (1990), with constants from Rodi (1985).

Initially χ is set to a background concentration. Values of $\overline{\theta_v'\chi'}$ are initialised to zero as conditions are thermally stable, and if counter-gradient fluxes are assumed unimportant for a particular simulation, the solution of equation (12) is omitted and $\overline{\theta_v'\chi'}$ is set to zero. Generally, counter-gradient fluxes are only important for near-source diffusion of point sources, and only when the model resolution is fine enough (less than 1 km) to resolve near-source concentrations adequately.

For pollutant concentration at inflow boundaries on the outermost grid, a background concentration is specified, while values at the boundaries of inner grids are obtained from the previous nest. At outflow boundaries, zero gradient boundary conditions are used. Zero gradient boundary conditions are used for $\overline{\theta_v'\chi'}$ on all grids.

3.1.2 Chemistry

Gas-phase photochemistry is based on the semi-empirical mechanism called the Generic Reaction Set (GRS) of Azzi *et al*. (1992), with the hydrogen peroxide modification of Venkatram *et al*. (1997). We have also included gas- and aqueous-phase reactions of sulfur dioxide and particles, with the aqueous-phase reactions based on Seinfeld and Pandis (1998).

There are ten reactions for twelve species: smog reactivity (R_{smog}), the radical pool (RP), hydrogen peroxide (H_2O_2), nitric oxide (NO), nitrogen dioxide (NO_2), ozone (O_3), sulfur dioxide (SO_2), stable non-gaseous organic carbon (SNGOC), stable gaseous nitrogen products (SGN), stable non-gaseous nitrogen products (SNGN), stable non-gaseous sulfur products (SNGS), and Airborne Particulate Matter (APM) which includes secondary particulate concentrations consisting of (SNGOC), (SNGN), and (SNGS).

The reactions are

Reactions	*Reaction Rates*
$R_{smog} + h\nu \rightarrow RP + R_{smog} + \eta SNGOC$	$R_1 = k_1[R_{smog}]$
$RP + NO \rightarrow NO_2$	$R_2 = k_2[RP][NO]$
$NO_2 + h\nu \rightarrow NO + O_3$	$R_3 = k_3[NO_2]$
$NO + O_3 \rightarrow NO_2$	$R_4 = k_4[NO][O_3]$
$RP + RP \rightarrow RP + \alpha H_2O_2$	$R_5 = k_5[RP][RP]$
$RP + NO_2 \rightarrow SGN$	$R_6 = k_6[RP][NO_2]$
$RP + NO_2 \rightarrow SNGN$	$R_7 = k_7[RP][NO_2]$
$RP + SO_2 \rightarrow SNGS$	$R_8 = k_8[RP][SO_2]$
$H_2O_2 + SO_2 \rightarrow SNGS$	$R_9 = k_9[H_2O_2][SO_2]$
$O_3 + SO_2 \rightarrow SNGS$	$R_{10} = k_{10}[O_3][SO_2]$

where [A] denotes concentration of species A and hv denotes ultra-violet radiation.

Yield coefficients are

$$\alpha = \max\left(0.03, \exp\left(-0.0261\frac{[R_{smog}]}{[NO_X]}\right)\right),$$

$$\eta = 0.1,$$

and reaction rate coefficients are

$$k_1 = k_3 f,$$
$$k_2 = 3580/(60T),$$
$$k_3 = 0.0001\delta.TSR/60,$$
$$k_4 = (924/60T)\exp(-1450/T),$$
$$k_5 = (1000/60),$$
$$k_6 = (0.12/60),$$
$$k_7 = k_6,$$
$$k_8 = 0.1k_7,$$

$$k_9 = \frac{7.45\times10^7[H^+]\alpha_1}{1+13[H^+]}K_{H\_S(IV)}K_{H\_H_2O_2}L.R.T.10^{-9},$$

$$k_{10} = (2.4\times10^4\alpha_0 + 3.7\times10^5\alpha_1 + 1.5\times10^9\alpha_2)K_{H\_S(IV)}K_{H\_O_3}L.R.T.10^{-9},$$

with

$$[H^+] = 10^{-pH},$$

$$\alpha_0 = \frac{K_{H0\_SO_2}}{K_{H\_S(IV)}}, \alpha_1 = \alpha_0\frac{K_{H1\_SO_2}}{[H^+]}, \alpha_2 = \alpha_1\frac{K_{H2\_SO_2}}{[H^+]},$$

$$K_{H\_S(IV)} = K_{H0\_SO_2}\left(1+\frac{K_{H1\_SO_2}}{[H^+]}\left(1+\frac{K_{H2\_SO_2}}{[H^+]}\right)\right),$$

$$K_{H0\_SO_2} = 1.24\exp\left(-3120\left(\frac{1}{298}-\frac{1}{T}\right)\right),$$

$$K_{H1\_SO_2} = 1.29\times10^{-2}\exp\left(-2080\left(\frac{1}{298}-\frac{1}{T}\right)\right),$$

$$K_{H2\_SO_2} = 6.014\times10^{-8}\exp\left(-1120\left(\frac{1}{298}-\frac{1}{T}\right)\right),$$

$$K_{H\_H_2O_2} = 7.1\times10^4\exp\left(-7250\left(\frac{1}{298}-\frac{1}{T}\right)\right),$$

$$K_{H\_O_3} = 9.4\times10^{-3}\exp\left(-2520\left(\frac{1}{298}-\frac{1}{T}\right)\right),$$

(all $K_H \le (L.R.T)^{-1}$),

where APM is in μg m^{-3}, all other species are in units of ppb, the rate coefficients k_1, k_3 are in s^{-1} and $k_2, k_4, k_5, k_6, k_7, k_8, k_9, k_{10}$ are in ppb^{-1} s^{-1}, temperature T is in K, the total solar radiation TSR is in W m^{-2}, R is the gas constant (0.082) in atm M^{-1} K^{-1}, L is the volume based liquid water fraction related to the liquid water specific humidity by $L = q_L \rho / \rho_W$,

$$f = \exp\left(-4700\left(\frac{1}{T} - \frac{1}{316}\right)\right),$$

$$\delta = \begin{cases} 4.23 + 1.09 / \cos Z; & \text{if } 0 \le Z \le 47 \\ 5.82; & \text{if } 47 \le Z \le 64, \\ -0.997 + 12(1 - \cos Z); & \text{if } 64 \le Z \le 90 \end{cases}$$

and Z is the zenith angle in degrees.

The value of the yield factor η for SNGOC is a preliminary one, and needs to be determined more accurately from data. We have also increased the reaction rate for RP destruction k_5 over the value of Azzi (1992), in order to give realistic values for the gas-phase reaction of SO_2 in the absence of NO_X. This change had no significant effect on concentrations of other gases. The secondary formation of APM by the various processes is in a preliminary form here, and needs to be verified against appropriate data.

The concept of using R_{smog} rather than Volatile Organic Compounds (VOCs) in the reaction equations follows from the work of Johnson (1984). The concentration of R_{smog} is defined as a reactivity coefficient multiplied by VOC concentration. For example, Johnson (1984) has used $[R_{smog}] = 0.0067[VOC]$ for typical 1980's Australian urban air dominated by motor vehicles. Empirically determined reactivity coefficients for individual VOC species are available from smog chamber experiments, while numerically determined reactivity coefficients have been calculated by comparison of the GRS mechanism with more complex mechanisms (Cope, 1999, personal communication)

Table 2 : Characteristics of the CBIV lumped VOC species needed for the GRS mechanism (Cope, 1999, personal communication).

CBIV Lumped VOC Species (i)	Carbon Number (CN_i)	Molecular Weight (MW_i)	CBIV Reactivity (a_i) (ppb $ppbC^{-1}$)
Formaldehyde (FORM) (CH_20)	1	30	0.0174
Higher Aldehydes (ALD2) (C_2H_40)	2	44	-0.00081
Ethene (ETH) (C_2H_4)	2	28	0.0153
Alkenes (Olefins) (OLE) (C_2H_4)	2	28	0.0127
Alkanes (Paraffins) (PAR) (CH_2)	1	14	0.00095
Toluene (TOL) (C_7H_8)	7	92	0.0049
Xylene (XYL) (C_8H_{10})	8	106	0.0145
Isoprene (ISOP) (C_5H_8)	5	68	0.0092

Emissions from VOC sources usually consist of more than one type of VOC, necessitating the R_{smog} emission rate to be calculated in the following way

$$Q_{Rsmog} = \sum_i \frac{14CN_i}{MW_i} a_i Q_i \ ,$$

where Q_i is the emission rate (g s^{-1}) for each VOC, a_i is its reactivity, CN_i is its carbon number and MW_i is its molecular weight. An alternative (and more precise) approach is to use a standard reactivity coefficient for a standard VOC mixture (for example $Q_{Rsmog} = 0.0064 Q_{VOC}$) with perturbations about this standard accounted for using the individual species reactivity coefficients (Cope, 1999, personal communication). Sample perturbation coefficients for the Carbon Bond IV (CBIV) mechanism are summarised in Table 2.

If we define $[NO_X] = [NO] + [NO_2]$ and $[SP_X] = [O_3] + [NO_2]$ (analogous to the definition of Smog Produced by Johnson, 1984, but without including SGN and SNGN), we do not need the differential equations for NO and O_3. The resulting reaction terms for the prognostic equation (11) for the eight pollutants APM, SO_2, NO_X, R_{smog}, SP_X, NO_2, RP, and H_2O_2 are

$$R_{[APM]} = F_{CH2}\eta R_1 + F_{HNO3} R_7 + F_{H2SO4}\left(R_8 + R_9 + R_{10}\right)$$
$$R_{[SO_2]} = -R_8 - R_9 - R_{10}$$
$$R_{[NO_X]} = -R_6 - R_7$$
$$R_{[R_{smog}]} = 0$$
$$R_{[SP_X]} = R_2 - R_6 - R_7 - R_{10}$$
$$R_{[NO_2]} = R_2 - R_3 + R_4 - R_6 - R_7$$
$$R_{[RP]} = R_1 - R_2 - R_5 - R_6 - R_7 - R_8$$
$$R_{[H_2O_2]} = \alpha R_5 - R_9$$

where $F_{HNO3} = 2.6, F_{H2SO4} = 4.0, F_{CH2} = 0.57$, are approximate factors to convert the stable non-gaseous compounds to APM in µg m^{-3} at NTP.

The potentially fast reactions in the reduced system are for SO_2, NO_2, RP, and H_2O_2. This implies that a small explicit timestep is necessary, but this restriction can be overcome by using a simple implicit solution procedure described later. This approach then allows large numerical time-steps to be used, provided the pH of the liquid water present is below about 5.5 (so that the reaction between O_3 and SO_2 to produce SNGS (R_{10}) does not dominate the aqueous phase reactions). Note that the default pH of the liquid water present in the model is 4.5, which is typical of Australian conditions.

3.1.3 Deposition

The dry deposition formulation for pollutants follows that of Physick (1994) in which all scalars behave like heat in terms of roughness length and stability function. Knowing the resistance functions for heat transfer r_{aH} and r_{bH} (Section 2.6.3), and the stomatal resistance r_S (Section 2.6.2), the surface flux for variable χ is written as $\overline{w'\chi'}\big|_o = -\chi_1 V_d$,

where the deposition velocity is $V_d = \left(r_{aero} + r_{surface}\right)^{-1}$, the aerodynamic resistance is $r_{aero} = r_{aH} + r_{bH}\left(D_w / D_\chi\right)^{2/3}$, the surface resistance $r_{surface}$ depends on the surface type, and

D_w and D_χ are molecular diffusivities for water vapour and pollutant concentration respectively.

For a land surface, $V_d = \dfrac{\sigma_f \beta}{r_{aero} + r_{water}} + \dfrac{\sigma_f (1-\beta)}{r_{aero} + r_S (D_w / D_\chi)} + \dfrac{(1-\sigma_f)}{r_{aero} + r_{soil}}$

and for a water surface, $V_d = \dfrac{1}{r_{aero} + r_{water}}$.

Non-zero deposition velocities are used for the pollutants APM, NO_2, NO, O_3, SO_2 and H_2O_2, with resistance values based on information in Wesley (1989), Harley *et al*. (1993) and Manins *et al*. (1996)

APM: $r_{water} = 0, r_{soil} = 1000, D_w / D_{APM} = 1.0$;

NO_2: $r_{water} = 500, r_{soil} = 500, D_w / D_{NO2} = 1.6$;

NO: $r_{water} = 500, r_{soil} = 5000, D_w / D_{NO} = 1.3$;

O_3: $r_{water} = 2000, r_{soil} = 300, D_w / D_{O3} = 1.6$;

SO_2: $r_{water} = 0, r_{soil} = 500, D_w / D_{SO2} = 1.9$;

H_2O_2: $r_{water} = 0, r_{soil} = 100, D_w / D_{H2O2} = 1.4$.

Wet deposition is important only for highly soluble gases and particles. For the pollutants considered in this model, the only ones removed by wet processes are APM, SO_2, and H_2O_2.

For the gases SO_2 and H_2O_2, the amount of each pollutant dissolved in the rain-water fraction of the liquid water is computed for pollutant A as $[A]_R = (L_R R T K_{H\_A})[A]$, where $L_R = q_R \rho / \rho_W$ is the liquid rain-water volume fraction, R is the gas constant (0.082) in atm M^{-1} K^{-1}, T is temperature in K, K_{H_A} is the effective Henry's Law coefficient for A, and concentrations are in ppb. $[A]_R$ is then vertically advected at the speed of the falling rain (V_T), to give $[A]_{R(NEW)}$. The new value of A is then $[A]_{(NEW)} = [A] - [A]_R + [A]_{R(NEW)}$.

For APM, the same approach is used as for the gases, except that we assume $K_{H\_A} = K_{H\_MAX} = (L_T R T)^{-1}$ (ie: that all particles are dissolved in the available water), with the total liquid water volume fraction $L_T = (q_C + q_R)\rho / \rho_W$.

3.2 Lagrangian particle module

The Lagrangian Particle Module (LPM) can be used on the inner-most nest for selected point sources to allow a more detailed account of near-source effects, including gradual plume rise and near-source dispersion. The LPM uses a PARTPUFF approach as described by Hurley (1994), whereby mass is represented as a puff in the horizontal direction, and as a particle in the vertical direction. This configuration has been used successfully in the Lagrangian Atmospheric Dispersion Model (LADM, Physick *et al.*, 1994). Chemistry is accounted for in a straightforward coupled manner with the EGM, without having to convert secondary pollutant concentration back to particle mass. This is done by tracking primary emissions for a particular source with the LPM and accounting for reactions using the EGM (see later). Deposition processes are neglected in the LPM. Once particles have travelled for a certain length of time (model input), the particle is no longer tracked and its mass is converted to concentration and put onto the EGM grid.

3.2.1 Pollutant equations

In the horizontal directions, particle position is updated through advection by the ambient wind, with diffusion accounted for through a puff width relation based on statistical diffusion theory

$$\frac{d\sigma_y^2}{dt} = 2\left(\sigma_u^2 + \sigma_{up}^2\right) T_{Lu}\left(1 - \exp\left(-\frac{t}{T_{Lu}}\right)\right),$$

where

$\sigma_u^2, \sigma_{up}^2$ are the ambient and plume rise horizontal velocity variances respectively,

$\sigma_u^2 = E - \frac{1}{2}\overline{w'^2}$,

σ_{up}^2 is specified in Section 3.3,

$T_{Lu} = \dfrac{2\sigma_u^2}{C_0 \varepsilon}$ is the ambient horizontal Lagrangian timescale,

and $C_0 = 2.0$.

In the vertical direction, particle position is updated using

$$\frac{d\sigma_{particle}}{dt} = \dot{\sigma} + \dot{\sigma}' + \dot{\sigma}'_p,$$

where

$\sigma_{particle}$ is the particle position in terrain following coordinates,

$\dot{\sigma}$ is the mean ambient vertical velocity,

$\dot{\sigma}'$ is the perturbation of vertical velocity due to ambient turbulence,

$\dot{\sigma}'_p$ is the perturbation of vertical velocity due to plume rise effects.

Perfect reflection of particle vertical position and velocity is used at the ground.

The perturbation of vertical velocity due to ambient turbulence is determined from the solution of a Langevin equation using a non-stationary turbulence extension of the approach of Franzese *et al.* (1999)

$$\dot{\sigma}' = w' \frac{\partial \sigma}{\partial z},$$

$$dw' = (a_0 + a_1 w' + a_2 w'^2)dt + b_0 \xi,$$

where ξ is a random number from a Gaussian distribution with mean zero and variance one, and

$$b_0 = \sqrt{C_0 \varepsilon dt},$$

$$a_2 = \frac{\frac{1}{3}\left(\frac{\partial \overline{w'^3}}{\partial t} + \frac{\partial \overline{w'^4}}{\partial z}\right) - \frac{\overline{w'^3}}{2\overline{w'^2}}\left(\frac{\partial \overline{w'^2}}{\partial t} + \frac{\partial \overline{w'^3}}{\partial z} - C_0\varepsilon\right) - \overline{w'^2}\frac{\partial \overline{w'^2}}{\partial z}}{\overline{w'^4} + \frac{\left(\overline{w'^3}\right)^2}{\overline{w'^2}} + \left(\overline{w'^2}\right)^2},$$

$$a_1 = \frac{1}{2\overline{w'^2}}\left(\frac{\partial \overline{w'^2}}{\partial t} + \frac{\partial \overline{w'^3}}{\partial z} - C_0\varepsilon - 2\overline{w'^3}a_2\right),$$

$$a_0 = \frac{\partial \overline{w'^2}}{\partial z} - \overline{w'^2}a_2.$$

Vertical velocity variance $\overline{w'^2}$ can be diagnosed from the following modified prognostic equation of Gibson and Launder (1978) and Andren (1990), when all advection and diffusion terms are neglected and the boundary layer assumption is made (see Mellor and Yamada, 1982),

$$\overline{w'^2} = \left(\tfrac{2}{3}E + \frac{E}{c_{s1}\varepsilon}\left((2 - c_{s2} - c_{w2}\frac{l}{kz})P_s + (2 - c_{s3} - c_{w3}\frac{l}{kz})P_b - \tfrac{2}{3}\varepsilon\right)\right).\left(1 + \frac{c_{w1}}{c_{s1}}\frac{l}{kz}\right)^{-1},$$

with constants from Rodi (1985)

$c_{s1} = 2.20,\ c_{s2} = 1.63,\ c_{s3} = 0.73,\ c_{w1} = 1.00,\ c_{w2} = 0.24,\ c_{w3} = 0.0$.

Higher-order moments of the vertical velocity distribution $\overline{w'^3}$ and $\overline{w'^4}$ are determined from the vertical velocity variance using

$$\overline{w'^3} = 0.8\left(\max\left(0, \overline{w'^2} - \overline{w_1'^2}\right)\right)^{3/2},$$

$$\overline{w'^4} = 3.5\left(\overline{w'^2}\right)^2,$$

in the convective boundary layer, and Gaussian values used elsewhere

$$\overline{w'^3} = 0.0,$$

$$\overline{w'^4} = 3.0\left(\overline{w'^2}\right)^2.$$

The subscript 1 here refers to the value of this variable at the first model level (10 m). This parameterisation produces a skewness of zero at the bottom and top of the convective boundary layer, and a peak value of about 0.6 within this layer. These parameterisations agree with measurements in the convective boundary layer as discussed by Luhar *et al.* (1996).

The perturbation of vertical velocity due to plume rise effects is determined using a random walk approach

$$\dot{\sigma}_p' = \left(w_p + \xi\sigma_{wp}\right)\frac{\partial\sigma}{\partial z},$$

where ξ is a random number from a Gaussian distribution with mean zero and variance one, and plume rise variables w_p and σ_{wp} are defined in Section 3.3.

In order to calculate total pollutant concentration for use in chemistry calculations and time-averaging, particles are converted to concentration at grid points of the EGM using the equation for the concentration increment of a particle at a grid point

$$\Delta\chi = \frac{\Delta m}{2\pi_c\sigma_y^2\Delta z}\exp\left(-\frac{r^2}{2\sigma_y^2}\right),$$

where

Δm is the particle mass,

σ_y is the standard deviation of horizontal puff width,

Δz is the vertical grid spacing,

r is the horizontal distance from the particle position to the grid point.

3.2.2 Chemistry

Pollutant emissions are converted to particle mass on release from the source, and stored for the variables APM, SO_2, NO_X, R_{smog}, SP_X and NO_2. Chemistry is accounted for in these variables by the EGM, except for the loss terms in the equation for SO_2, which are handled through an exponential decay of mass with reaction rate $k_{SO2} = k_8[RP] + k_9[H_2O_2] + k_{10}[O_3]$. This reaction is then not computed in the EGM for the LPM component of SO_2. This approach allows the dispersion of the primary emissions of the above variables to be handled with the LPM, and avoids any dependence of the LPM on the EGM, except for the first order reaction rate of SO_2.

The diagnostic solution for the total concentration is then

$$[APM] = [APM]_{LPM} + [APM]_{EGM},$$
$$[SO_2] = [SO_2]_{LPM} + [SO_2]_{EGM},$$
$$[NO_X] = [NO_X]_{LPM} + [NO_X]_{EGM},$$
$$[R_{smog}] = [R_{smog}]_{LPM} + [R_{smog}]_{EGM},$$
$$[SP_X] = [SP_X]_{LPM} + [SP_X]_{EGM},$$
$$[NO_2] = [NO_2]_{LPM} + [NO_2]_{EGM},$$
$$[RP] = [RP]_{EGM},$$
$$[H_2O_2] = [H_2O_2]_{EGM}.$$

3.3 Plume rise module

The equations for mean plume rise of a point source emission are based on the model of Glendening *et al*. (1984), as simplified by Hurley and Manins (1995)

$$\frac{dG}{dt} = 2R\left(\alpha w_p^2 + \beta u_a w_p + \gamma u_p E^{1/2}\right),$$
$$\frac{dF}{dt} = -\frac{sM}{u_p}\left(\frac{M}{M_{eff}} u_a + w_p\right),$$
$$\frac{dM}{dt} = F,$$
$$\frac{dx_p}{dt} = u,$$
$$\frac{dy_p}{dt} = v,$$
$$\frac{dz_p}{dt} = w_p,$$

with

$G = \frac{T_a}{T_p} u_p R^2,$

$F = g u_p R^2 \left(1 - \frac{T_a}{T_p}\right),$

$M = \frac{T_a}{T_p} u_p R^2 w_p,$

$w_p = \frac{M}{G},$

$R = \sqrt{\frac{(G + F/g)}{u_p}},$

$u_p = \sqrt{u_a^2 + w_p^2},$

$u_a = \sqrt{u^2 + v^2},$

G, F, M = plume volume, buoyancy, and momentum flux respectively,

R = plume radius (top - hat cross - section),

u, v, w = cartesian x, y, z components of velocity respectively,

T = temperature,

s = ambient buoyancy frequency,

subscript a refers to ambient variables, subscript p refers to plume variables,

$\alpha = 0.1$, $\beta = 0.6$, $\gamma = 0.1$, are vertical plume, bent - over plume, and ambient turbulence entrainment constants respectively,

$\frac{M}{M_{eff}} = \frac{1}{2.25}$, g = gravitational constant (9.8 m s^{-1}).

Initial conditions for these equations are

$$G_o = \frac{T_a}{T_s} w_s R_s^2,\ F_o = g w_s R_s^2 \left(1 - \frac{T_a}{T_s}\right),\ M_o = \frac{T_a}{T_s} w_s^2 R_s^2,\ R_o = \sqrt{\frac{w_s}{\sqrt{u_a^2 + w_s^2}}},$$

with subscript s representing stack exit conditions. Termination of rise conditions for determining final plume rise height are based on zero buoyancy flux, and equal plume and ambient dissipation rates.

Tests of these equations against both the full Glendening and the Briggs (1975) form of the plume rise equations by Hurley and Manins (1995), showed that the above form was just as good as the full Glendening form for all conditions. Our form also collapses to the Briggs form for a bent-over Boussinesq plume, and to the Briggs vertical plume model equations for zero ambient wind. It was also found that for very hot plumes in a bent-over plume situation, the Briggs form was very close to our form, even though the Boussinesq approximation was not strictly valid. This finding is probably due to the rapid decrease of plume temperature excess with travel time.

In the EGM, plume rise for a point source is accounted for by releasing pollutants at the effective source height as calculated by the above equations, with a plume depth that assumes a 2:1 horizontal to vertical plume shape, and that the plume radius for concentration is two-thirds that of the visual radius R above. Pollutant emissions are then distributed uniformly to grid points within the plume depth at the nearest horizontal grid point (assuming plume width is always sub-grid scale).

In the LPM, a gradual plume rise approach is used with a random component which depends on the standard deviation of the vertical velocity due to plume rise effects, and an enhanced horizontal spread. The standard deviations of velocity assume a slightly simplified form of the above equation for *G*, a 2:1 horizontal to vertical plume shape, a plume radius for concentration of two-thirds the visual radius *R*, and a standard deviation half that of the radius. This results in the equations

$$\sigma_{wp} = \frac{\alpha w_p^2 + \beta u_a w_p}{3\sqrt{2}u_p}, \text{ and } \sigma_{up} = 2\sigma_{wp}.$$

4 Numerical methods

The flow chart in Figure 1 illustrates the order of calculations in the model. The model uses a large timestep of 300 s on which radiation and surface processes are calculated. Meteorological and turbulence equations are solved with a timestep of $\Delta t_M = \frac{1}{U_M}\min(\Delta x_M, \Delta y_M)$, where U_M is a characteristic wind speed (U_M = 30 m s^{-1} is the model default), and Δx_M and Δy_M are the horizontal grid spacings in metres on the meteorological grid. Pollution concentration equations for the EGM are solved with a timestep of $\Delta t_P = \frac{1}{U_P}\min(\Delta x_P, \Delta y_P)$, where U_P =0.5U_M, and Δx_P and Δy_P are the horizontal grid spacings in metres on the pollution grid. The pollution grid can be a subset of the meteorological grid at finer grid spacing. The maximum synoptic wind speed used by the model is set to be U_M, in order to avoid Courant numbers being too much greater than 1 for the meteorology. This restriction was found to be important for the reduction of numerical error, particularly near the model top and in non-hydrostatic mode.

Model equations are solved using finite difference methods with no grid stagger, a constant grid spacing in the horizontal directions, and a variable grid spacing in the vertical direction. Second-order centred spatial differencing is used, for example

$$\left.\frac{\partial\phi}{\partial x}\right|_i = \frac{1}{2\Delta x}(\phi_{i+1} - \phi_{i-1}),$$

$$\left.\frac{\partial\phi}{\partial y}\right|_j = \frac{1}{2\Delta y}(\phi_{j+1} - \phi_{j-1}),$$

$$\left.\frac{\partial\phi}{\partial\sigma}\right|_k = \frac{1}{(\sigma_{k+1} - \sigma_{k-1})}\left(\left(\frac{\sigma_k - \sigma_{k-1}}{\sigma_{k+1} - \sigma_k}\right)(\phi_{k+1} - \phi_k) + \left(\frac{\sigma_{k+1} - \sigma_k}{\sigma_k - \sigma_{k-1}}\right)(\phi_k - \phi_{k-1})\right),$$

$$\left.\frac{\partial}{\partial x}\left(K\frac{\partial\phi}{\partial x}\right)\right|_i = \frac{1}{2(\Delta x)^2}\left((K_{i+1} + K_i)(\phi_{i+1} - \phi_i) - (K_i + K_{i-1})(\phi_i - \phi_{i-1})\right),$$

$$\left.\frac{\partial}{\partial y}\left(K\frac{\partial\phi}{\partial y}\right)\right|_j = \frac{1}{2(\Delta y)^2}\left((K_{j+1} + K_j)(\phi_{j+1} - \phi_j) - (K_j + K_{j-1})(\phi_j - \phi_{j-1})\right),$$

$$\left.\frac{\partial}{\partial\sigma}\left(K\frac{\partial\phi}{\partial\sigma}\right)\right|_k = \frac{1}{(\sigma_{k+1} - \sigma_{k-1})}\left(\left(\frac{K_{k+1} + K_k}{\sigma_{k+1} - \sigma_k}\right)(\phi_{k+1} - \phi_k) - \left(\frac{K_k + K_{k-1}}{\sigma_k - \sigma_{k-1}}\right)(\phi_k - \phi_{k-1})\right).$$

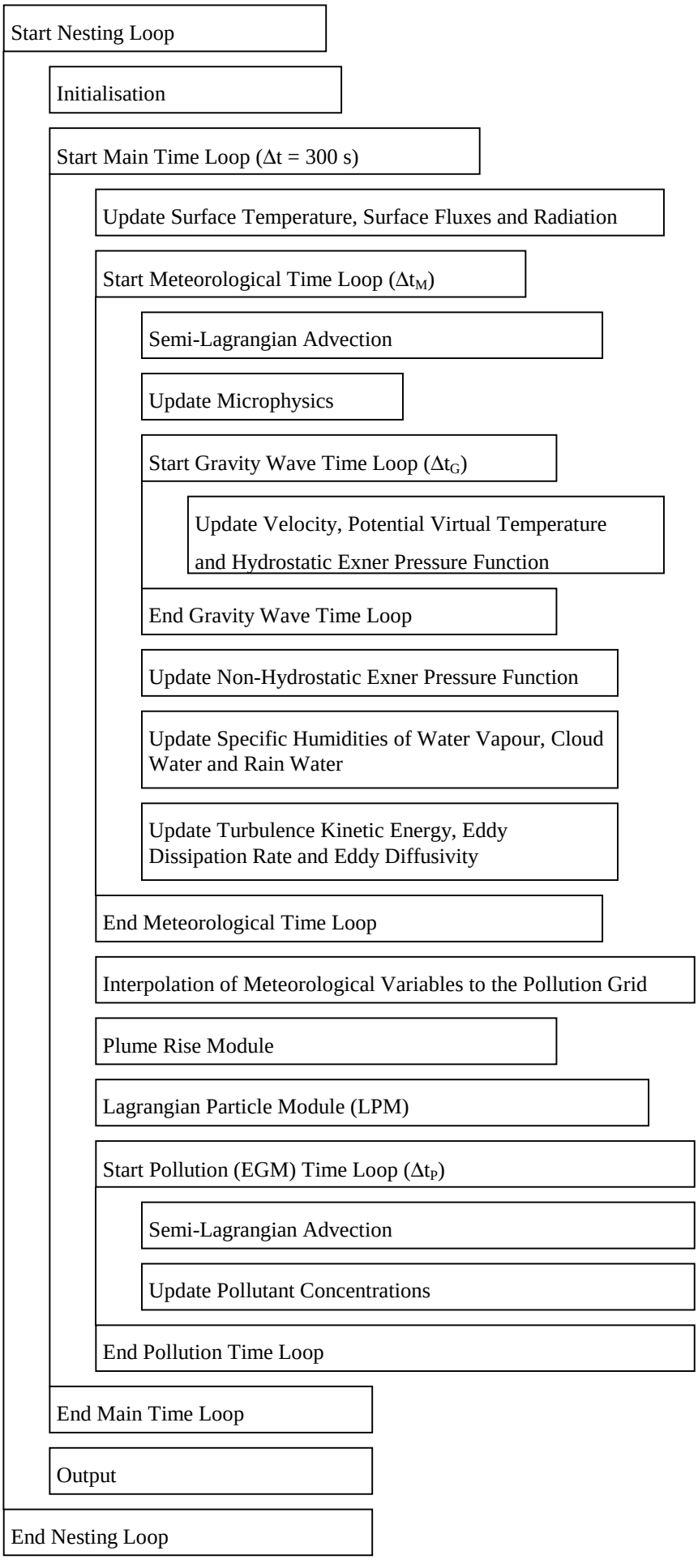

Figure 1. Flow chart of TAPM.

4.1 Horizontal advection

Horizontal advection for all prognostic variables is calculated with timesteps Δt_M or Δt_P using the semi-Lagrangian technique of McGregor (1993) with the quasi-monotone conversion of Bermejo and Staniforth (1992). To $O((\Delta t)^2)$, the departure point (i_*, j_*) in grid units can be determined for horizontal grid point (i, j) from

$$i_* = i - u_{i,j}^{n+1/2}\frac{\Delta t}{\Delta x} + \frac{(\Delta t)^2}{2\Delta x}\left(u\frac{\partial u}{\partial x} + v\frac{\partial u}{\partial y}\right)\Bigg|_{i,j}^{n+1/2},$$

$$j_* = j - v_{i,j}^{n+1/2}\frac{\Delta t}{\Delta y} + \frac{(\Delta t)^2}{2\Delta y}\left(u\frac{\partial u}{\partial x} + v\frac{\partial u}{\partial y}\right)\Bigg|_{i,j}^{n+1/2},$$

with $u_{i,j}^{n+1/2} = 1.5u_{i,j}^{n} - 0.5u_{i,j}^{n-1}$ or $u_{i,j}^{n+f} = fu_{i,j}^{n+1} + (1-f)u_{i,j}^{n}$ and similarly for v, for the meteorological and concentration variables respectively (f accounts for fractional timesteps). Each prognostic variable can then be determined from $\phi_{i,j}^{n+1} = \phi_{i_*,j_*}^{n}$ using Lagrange cubic polynomial interpolation separately in each coordinate direction.

Defining $i = \text{int}(i_*)$ and $x_* = i_* - i$, then

$$\phi_{i_*j}^{n} = -\tfrac{1}{6}x_*(x_*-1)(x_*-2)\phi_{i-1j}^{n} + \tfrac{1}{2}(x_*^2-1)(x_*-2)\phi_{ij}^{n} - \tfrac{1}{2}x_*(x_*+1)(x_*-2)\phi_{i+1j}^{n} + \tfrac{1}{6}x_*(x_*^2-1)\phi_{i+2j}^{n},$$

subject to $\min(\phi_{ij}^{n}, \phi_{i+1j}^{n}) \le \phi_{i_*j}^{n} \le \max(\phi_{ij}^{n}, \phi_{i+1j}^{n})$.

Similarly, if $j = \text{int}(j_*)$ and $y_* = j_* - j$, then

$$\phi_{i_*j_*}^{n} = -\tfrac{1}{6}y_*(y_*-1)(y_*-2)\phi_{i_*j-1}^{n} + \tfrac{1}{2}(y_*^2-1)(y_*-2)\phi_{i_*j}^{n} - \tfrac{1}{2}y_*(y_*+1)(y_*-2)\phi_{i_*j+1}^{n} + \tfrac{1}{6}y_*(y_*^2-1)\phi_{i_*j+2}^{n},$$

subject to $\min(\phi_{i_*j}^{n}, \phi_{i_*j+1}^{n}) \le \phi_{i_*j_*}^{n} \le \max(\phi_{i_*j}^{n}, \phi_{i_*j+1}^{n})$.

4.2 Vertical advection

Vertical advection for all prognostic variables except θ_v, is calculated with timesteps Δt_M or Δt_P using the semi-Lagrangian technique of McGregor (1993) with the quasi-monotone conversion of Bermejo and Staniforth (1992). To $O((\Delta t)^2)$, the departure point can be determined from

$$\sigma_* = \sigma_k - \dot{\sigma}_k^{n+1/2}\Delta t + \tfrac{1}{2}(\Delta t)^2\left(\dot{\sigma}\frac{\partial\dot{\sigma}}{\partial\sigma}\right)\Bigg|_{k}^{n+1/2},$$

with $\dot{\sigma}_k^{n+1/2} = 1.5\dot{\sigma}_k^{n} - 0.5\dot{\sigma}_k^{n-1}$ or $\dot{\sigma}_k^{n+f} = f\dot{\sigma}_k^{n+1} + (1-f)\dot{\sigma}_k^{n}$, for the meteorological and concentration variables respectively (f accounts for fractional timesteps). Each prognostic variable can then be determined from $\phi_k^{n+1} = \phi_{k_*}^{n}$ (where k denotes the nearest model level to σ_* that satisfies $\sigma_k \le \sigma_*$), using Lagrange cubic polynomial interpolation (with quasi-monotone conversion)

$$\phi^n_{k_*} = \left(\frac{\sigma_* - \sigma_k}{\sigma_{k-1} - \sigma_k}\right)\left(\frac{\sigma_* - \sigma_{k+1}}{\sigma_{k-1} - \sigma_{k+1}}\right)\left(\frac{\sigma_* - \sigma_{k+2}}{\sigma_{k-1} - \sigma_{k+2}}\right)\phi^n_{k-1}$$
$$+\left(\frac{\sigma_* - \sigma_{k-1}}{\sigma_k - \sigma_{k-1}}\right)\left(\frac{\sigma_* - \sigma_{k+1}}{\sigma_k - \sigma_{k+1}}\right)\left(\frac{\sigma_* - \sigma_{k+2}}{\sigma_k - \sigma_{k+2}}\right)\phi^n_k$$
$$+\left(\frac{\sigma_* - \sigma_{k-1}}{\sigma_{k+1} - \sigma_{k-1}}\right)\left(\frac{\sigma_* - \sigma_k}{\sigma_{k+1} - \sigma_k}\right)\left(\frac{\sigma_* - \sigma_{k+2}}{\sigma_{k+1} - \sigma_{k+2}}\right)\phi^n_{k+1}$$
$$+\left(\frac{\sigma_* - \sigma_{k-1}}{\sigma_{k+2} - \sigma_{k-1}}\right)\left(\frac{\sigma_* - \sigma_k}{\sigma_{k+2} - \sigma_k}\right)\left(\frac{\sigma_* - \sigma_{k+1}}{\sigma_{k+2} - \sigma_{k+1}}\right)\phi^n_{k+2},$$

subject to $\min(\phi^n_k, \phi^n_{k+1}) \le \phi^n_{k_*} \le \max(\phi^n_k, \phi^n_{k+1})$.

4.3 Gravity waves

The equations for the meteorological variables u, v, $\dot{\sigma}$, θ_v, and π_H are solved by using a time-split approach where gravity wave terms are separated from the others and solved on a small timestep $\Delta t_M = \frac{1}{U_G}\min(\Delta x_M, \Delta y_M)$, where U_G = 120 m s^{-1}.

$$\frac{\partial u}{\partial t} = -\theta_v \frac{\partial \pi_H}{\partial x} + R_u,$$
$$\frac{\partial v}{\partial t} = -\theta_v \frac{\partial \pi_H}{\partial y} + R_v,$$
$$\frac{\partial \dot{\sigma}}{\partial \sigma} = -\left(\frac{\partial u}{\partial x} + \frac{\partial v}{\partial y}\right) + u\frac{\partial^2 \sigma}{\partial \sigma \partial x} + v\frac{\partial^2 \sigma}{\partial \sigma \partial y},$$
$$\frac{\partial \theta_v}{\partial t} = -\dot{\sigma}\frac{\partial \theta_v}{\partial \sigma} + R_{\theta_v},$$
$$\frac{\partial \pi_H}{\partial \sigma} = -\frac{g}{\theta_v}\left(\frac{\partial \sigma}{\partial z}\right)^{-1},$$

with R_u, R_v, and R_{θ_v} (updated on the timestep Δt_M)

$$R_u = g\frac{\partial \sigma}{\partial x}\left(\frac{\partial \sigma}{\partial z}\right)^{-1} + f(v - v_s) - N_s(u - u_s) - \theta_v\left(\frac{\partial \pi_N}{\partial x} + \frac{\partial \pi_N}{\partial \sigma}\frac{\partial \sigma}{\partial x}\right),$$
$$R_v = g\frac{\partial \sigma}{\partial y}\left(\frac{\partial \sigma}{\partial z}\right)^{-1} - f(u - u_s) - N_s(v - v_s) - \theta_v\left(\frac{\partial \pi_N}{\partial y} + \frac{\partial \pi_N}{\partial \sigma}\frac{\partial \sigma}{\partial y}\right),$$
$$R_{\theta_v} = S_{\theta_v} - \gamma_{cg}\frac{\partial K}{\partial \sigma}\frac{\partial \sigma}{\partial z} - N_s(\theta_v - \theta_{vs}),$$

and also include the nesting terms.

These prognostic equations are solved using the second-order Adams-Bashforth scheme

$$u^{n+1} = u^n + \frac{\Delta t}{2}\left(3\frac{\partial u}{\partial t}\bigg|^n - \frac{\partial u}{\partial t}\bigg|^{n-1}\right),$$

while diagnostic vertical integration using the trapezoidal rule is performed from the ground to the model top to obtain $\dot{\sigma}$, and from the model top to the ground to obtain π_H.

On the timestep Δt_G, an implicit tri-diagonal horizontal filter described by Pielke (1984) is used instead of horizontal diffusion. The filter, represented by $F(\phi)$ in equations 1, 2 and 4 of Section 2.1, is applied separately in each horizontal direction with a filter coefficient of δ=0.10 (increased values are used near the top of the model). The equations solved are

$$(1-\delta)\phi_{i-1j}^{n+1} + 2(1+\delta)\phi_{ij}^{n+1} + (1-\delta)\phi_{i+1j}^{n+1} = \phi_{i-1j}^{n} + 2\phi_{ij}^{n} + \phi_{i+1j}^{n},$$

$$(1-\delta)\phi_{ij-1}^{n+1} + 2(1+\delta)\phi_{ij}^{n+1} + (1-\delta)\phi_{ij+1}^{n+1} = \phi_{ij-1}^{n} + 2\phi_{ij}^{n} + \phi_{ij+1}^{n}.$$

On the timestep Δt_M, vertical diffusion is solved using a first-order implicit approach with special treatment of fluxes at the surface boundary (see next section).

4.4 Scalar prognostic equations

All other prognostic equations including those for specific humidities, turbulence, and pollutant concentrations are of the general form for variable χ

$$\frac{\partial \chi}{\partial t} = \left(\frac{\partial \sigma}{\partial z}\right)^2 \frac{\partial}{\partial \sigma}\left(K\frac{\partial \chi}{\partial \sigma}\right) + RHS_1 - \chi RHS_2.$$

This equation is solved using first-order time differencing with a semi-implicit approach to give the equation

$$(1+\Delta t RHS_2)\chi^{n+1} - \Delta t\left(\frac{\partial \sigma}{\partial z}\right)^2 \frac{\partial}{\partial \sigma}\left(K\frac{\partial \chi^{n+1}}{\partial \sigma}\right) = \chi^n + \Delta t RHS_1,$$

which can be solved as follows (with special treatment of fluxes at the surface) using a tri-diagonal solution method if second-order spatial differencing is used

$A\chi_{k-1}^{n+1} + B\chi_k^{n+1} + C\chi_{k+1}^{n+1} = D;$

if $k > 1$:

$$A = -\left(\frac{\partial \sigma}{\partial z}\right)^2 \frac{\Delta t}{(\sigma_{k+1} - \sigma_{k-1})}\left(\frac{K_k + K_{k-1}}{\sigma_k - \sigma_{k-1}}\right),$$

$$C = -\left(\frac{\partial \sigma}{\partial z}\right)^2 \frac{\Delta t}{(\sigma_{k+1} - \sigma_{k-1})}\left(\frac{K_{k+1} + K_k}{\sigma_{k+1} - \sigma_k}\right),$$

$$B = 1 + \Delta t RHS_2 - A - C,$$

$$D = \chi_k^n + \Delta t RHS_1;$$

if $k = 1$:

$$A = 0,$$

$$C = -\frac{1}{2}\left(\frac{\partial \sigma}{\partial z}\right)^2 \frac{\Delta t}{(\sigma_{3/2} - \sigma_0)}\left(\frac{K_2 + K_1}{\sigma_2 - \sigma_1}\right),$$

$$B = 1 + \Delta t RHS_2 - C,$$

$$D = \chi_1^n + \Delta t RHS_1 - \Delta t\left(\frac{\partial\sigma}{\partial z}\right)\frac{\text{flux}(\chi)}{(\sigma_{3/2} - \sigma_0)},$$

with $\text{flux}(\chi) = u_*\chi_*$ or $\text{flux}(\chi) = V_d\chi_1$.

The value of RHS_2 is non-zero only for the ε equation, the $\overline{\theta_v'\chi'}$ equations, and the SO_2, NO_2, RP and H_2O_2 pollutant concentration equations, where the loss terms are treated implicitly. The RHS_1 term includes all other terms in the particular prognostic equations, including explicit horizontal diffusion. The non-zero RHS_2 terms are

$$\varepsilon : RHS_2 = c_{\varepsilon 2}\frac{\varepsilon}{E},$$

$$\overline{\theta_v'\chi'} : RHS_2 = \frac{2}{c_\chi}\frac{\varepsilon}{E},$$

$$[SO_2] : RHS_2 = k_8[RP] + k_9[H_2O_2] + k_{10}[O_3],$$

$$[NO_2] : RHS_2 = k_3 + k_4([NO_X] + [SP_X] - [NO_2]),$$

$$[RP] : RHS_2 = k_2[NO] + k_5[RP] + (k_6 + k_7)[NO_2] + k_8[SO_2],$$

$$[H_2O_2] : RHS_2 = k_9[SO_2].$$

When the stability criterion for explicit horizontal diffusion of pollution variables is breached, the solution dynamically switches to an unconditionally stable implicit mode analogous to that used for vertical diffusion.

4.5 Other methods

- On the timestep Δt_M, the elliptic non-hydrostatic pressure perturbation equation is solved using an iterative approach. The solution is performed only for a sub-grid region which excludes the 5 edge grid points at the top and lateral boundaries, as these edge regions usually contain noisy solutions which can produce spurious vertical velocities to which the non-hydrostatic solution is highly sensitive.
- For numerical representation of the vertical fluxes, it is necessary to use a finite difference approximation consistent with that used for the vertical diffusion

$$\overline{w'\chi'}\Big|_k = -\tfrac{1}{2}(K_{k+1} + K_k)\left(\frac{\sigma_k - \sigma_{k-1}}{\sigma_{k+1} - \sigma_{k-1}}\right)\left(\frac{\chi_{k+1} - \chi_k}{\sigma_{k+1} - \sigma_k}\right)\left(\frac{\partial\sigma}{\partial z}\right)$$
$$-\tfrac{1}{2}(K_k + K_{k-1})\left(\frac{\sigma_{k+1} - \sigma_k}{\sigma_{k+1} - \sigma_{k-1}}\right)\left(\frac{\chi_k - \chi_{k-1}}{\sigma_k - \sigma_{k-1}}\right)\left(\frac{\partial\sigma}{\partial z}\right).$$

- At times of rapid variations in the surface temperature and specific humidity (such as just after sunrise), the surface heat balance approach used for vegetation can produce oscillations. Therefore, the vegetation temperature and moisture are time averaged using the current and previous values to prevent the oscillations.
- Linear interpolation is used to convert the synoptic-scale variables from the gridded analyses to the model;
- The plume rise equations are solved using the fourth-order Runge-Kutta method with a timestep of 1 second.

- The LPM uses explicit, forward in time finite differences and centred in space finite differences, with a large timestep of $\Delta t_{LPM} = 2\Delta t_P$ and a small timestep of 5 seconds for the solution in the vertical direction.
- The turbulence production/dissipation balance and wet processes are handled separately on a small timestep of 100 s.
- For multi-dimensional simulations, it was found necessary to bound the value of the length scale in order to keep the numerical solution stable for the ε prognostic equation. Also, the counter-gradient tracer flux and cross-correlation term are restricted to be zero in thermally stable regions, and are bounded elsewhere.

5 Example simulations

5.1 Meteorology at Cape Grim

The Cape Grim baseline air monitoring station is situated on the north-west corner of Tasmania (latitude, longitude)=(-40°41′, 144°41.5′). The station was set up to measure baseline values of chemicals in the atmosphere, and it also routinely measures winds at 10 m and 50 m above the ground, and temperature and humidity at screen level. The site is situated within a few hundred metres of the coastline both to the west and to the north, with a steep cliff at the coast to the west and a more gradual slope to the north. The station is approximately 95 m above sea level.

Table 3 : Statistics for TAPM simulation of December 1997 at Cape Grim for wind speed at 10 and 50 m above the ground (WS10, WS50); the x-component of the wind (U10, U50); the y-component of the wind (V10, V50); temperature (TEMP); and relative humidity (RH).

VARIABLE	NUMBER	MEAN_OBS	MEAN_MOD	STD_OBS	STD_MOD	CORR	RMSE	RMSE_S	RMSE_U	IOA	SKILL_E	SKILL_V	SKILL_R
WS10	744	9.4	5.9	4.2	2.3	0.72	4.64	4.37	1.57	0.64	0.37	0.54	1.10
WS50	744	9.6	7.3	4.3	2.8	0.76	3.66	3.15	1.86	0.75	0.43	0.66	0.85
U10	744	5.4	3.4	6.9	3.9	0.88	4.32	3.91	1.84	0.84	0.27	0.57	0.63
U50	744	4.6	4.1	7.0	4.9	0.89	3.43	2.66	2.18	0.91	0.31	0.70	0.49
V10	744	2.5	1.2	4.8	3.3	0.75	3.51	2.73	2.20	0.80	0.45	0.68	0.72
V50	744	2.6	1.6	5.8	4.2	0.76	3.91	2.80	2.73	0.84	0.47	0.73	0.67
TEMP	742	13.6	14.3	1.8	1.7	0.79	1.35	0.87	1.03	0.84	0.58	0.95	0.76
RH	744	75.4	79.3	9.1	10.4	0.26	12.5	7.5	10.0	0.54	1.10	1.13	1.37

KEY: OBS = Observations, MOD = Model Predictions, NUMBER = Number of hourly-averaged values used for the statistics, MEAN = Arithmetic mean, STD = Standard Deviation, CORR = Pearson Correlation Coefficient (0=no correlation,1=exact correlation), RMSE = Root Mean Square Error, RMSE_S = Systematic Root Mean Square Error, RMSE_U = Unsystematic Root Mean Square Error, IOA = Index of Agreement (0=no agreement, 1=perfect agreement), SKILL_E = (RMSE_U)/(STD_OBS) (<1 shows skill), SKILL_V = (STD_MOD)/(STD_OBS) (near to 1 shows skill), SKILL_R = (RMSE)/(STD_OBS) (<1 shows skill).

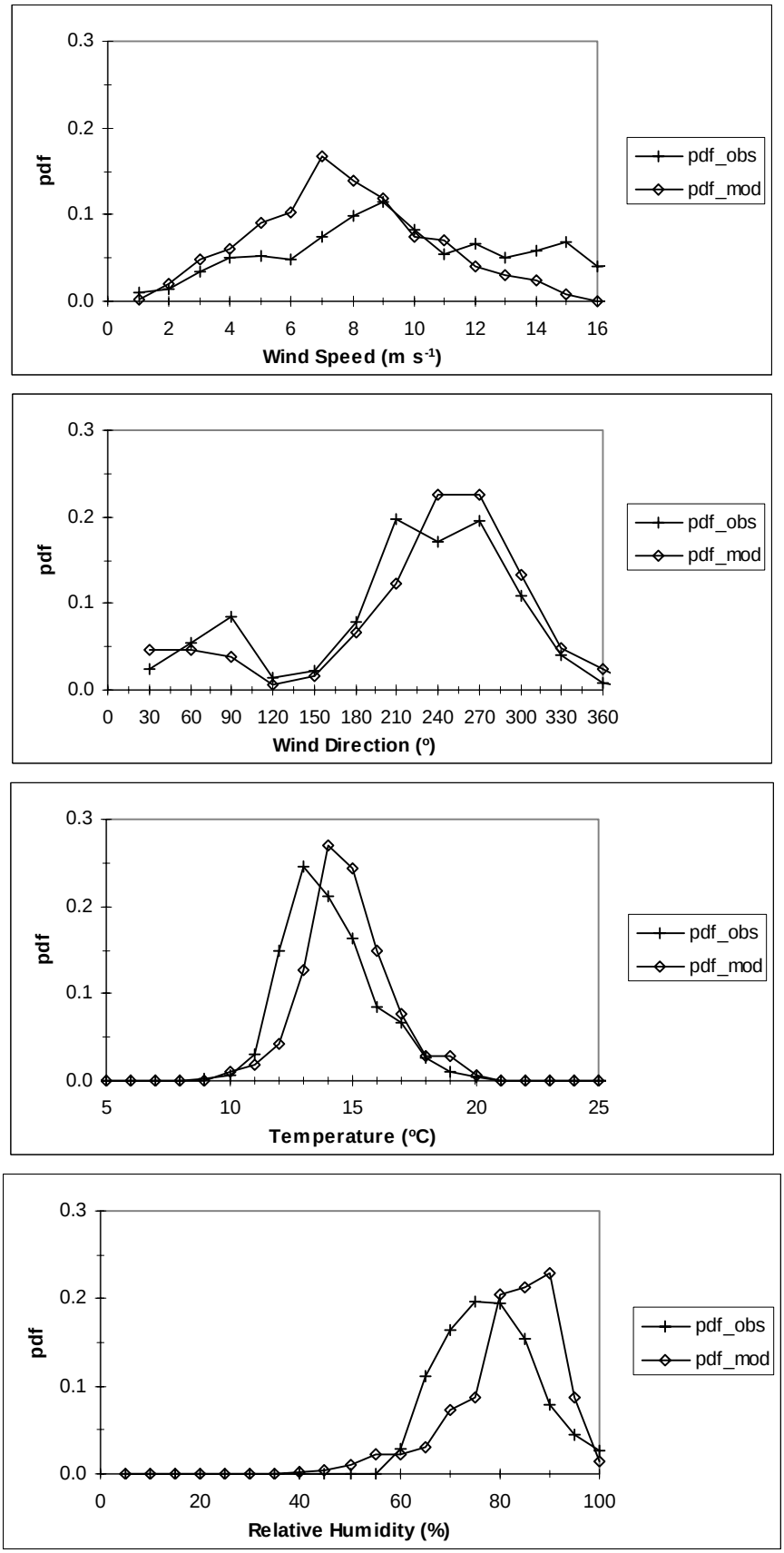

Figure 2 : Probability density functions (pdf) of observed (obs) and modelled (mod) wind speed and direction at 50 m and screen-level temperature and relative humidity.

TAPM was used to model the meteorology of December 1997 at Cape Grim, using as model input six hourly LAPS analysis data at a grid spacing of of 0.75° from the Bureau of Meteorology to provide the synoptic conditions (see Puri *et al*., 1998, for a description of LAPS), Rand's global sea surface temperatures from NCAR, 9 second DEM terrain height data from AUSLIG, and soil and vegetation classification data from CSIRO Wildlife and Ecology. The model was run with a triply nested grid of 30x30x20 points at 10,000 m, 3,000 m and 1,000 m horizontal grid spacing, with model options including time- and space-varying synoptic conditions, vegetation, rain, non-hydrostatic pressure, and $E-\varepsilon$ turbulence. The deep soil moisture content was set at 0.05 (dry), which is close to the wilting value for the sandy soil (type 1) that dominates the area. The dominant vegetation type was Grassland – mid-dense tussock (type 19).

Model predictions were extracted at the nearest grid point to the Cape Grim site on the inner grid (1,000 m spacing) at the lowest two model levels (10 m and 50 m above the ground). At this grid point the terrain height was 55 m above sea level. Statistics of observations and model predictions are shown in Table 3. The statistics used were based on the recommendations of Willmott (1981), and include the Index Of Agreement (IOA) which provides a more consistent measure of performance than the correlation coefficient (also shown for comparison). Probability density functions (pdfs) for winds at 50 m and temperature and relative humidity are shown in Figure 2.

Based on the Index of Agreement and the Skill Score statistics, the results suggest that temperature and 50 m level winds are predicted the best, while 10 m level wind speed and relative humidity are predicted less accurately. The mean wind speed was underestimated, particularly at the 10 m level, and the systematic component of the RMSE dominates the unsystematic component. This is perhaps not surprising given the complexity of the local-scale topography at Cape Grim which can lead to complex flow behaviour which the model (even at 1,000 m grid resolution) does not resolve. Baines and Murray (1991) illustrated this point with physical modelling of the flow behaviour at Cape Grim. They showed that under westerly synoptic winds the air reaching the measurement levels at the site were from a height of approximately 50 m higher upwind over the sea, so that the 50 m level on the tower was measuring air that had come from a height of 100 m. This coupled with the fact that the model terrain height used was approximately 45 m lower than the actual station elevation, could produce some underestimation of the wind speed. This is also evident in the comparison of mean u-component of the wind at 10 m.

Given the influence that the small-scale terrain effects have on the measurements, the model has performed well in predicting the observed meteorology in the Cape Grim region.

5.2 Dispersion in the convective boundary layer

In order to assess the model performance for pollutant concentration, a horizontally homogeneous meteorological situation was modelled for dispersion from a non-buoyant elevated point source. The synoptic meteorology was 5 m s^{-1} westerly wind with a simple temperature and humidity profile, and the non-buoyant source characteristics were a stack height of 300 m and an emission rate of 100 g s^{-1}. The model was run with a triply nested grid of 30x30x20 points at 10,000 m, 3,000 m and 1,000 m horizontal grid spacing, with pollution grids of 37x37x20 points covering the same corresponding areas as the meteorology at 2500 m, 750 m and 250 m horizontal grid spacing.

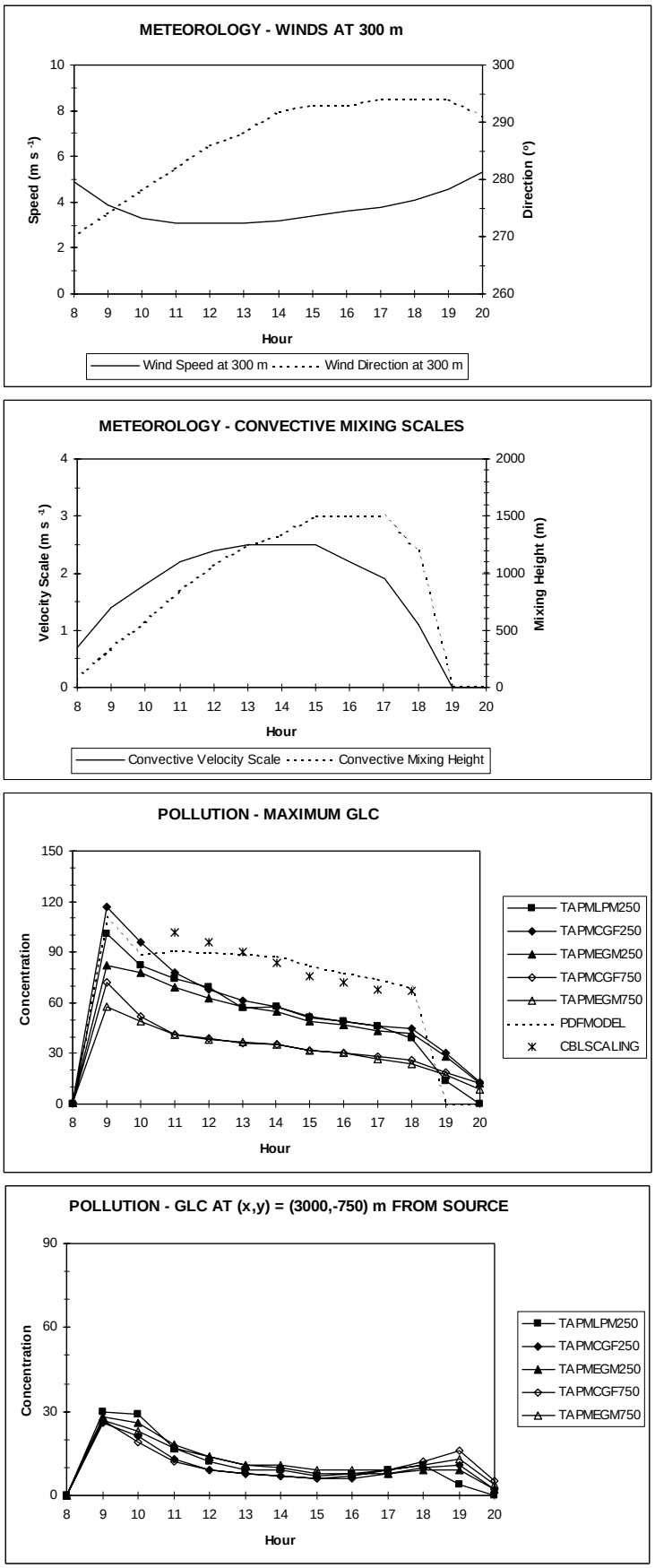

Figure 3 : Predicted meteorology and pollution ground level concentrations (glc) for elevated point source dispersion in a convective boundary layer.

Predicted winds at 300 m, convective mixing scales, the maximum ground level concentration (glc) in micrograms per cubic metre ($\mu g\ m^{-3}$), and the glc at the downwind point (x, y) = (3000, -750) m are shown in Figure 3. Several different pollution module options (EGM – the Eulerian Grid Module without counter gradient pollutant flux; CGF – the Eulerian Grid Module with counter gradient pollutant flux; LPM – the Lagrangian Particle Module) at two different pollutant grid spacings (750 m and 250 m) are shown to help identify the differences between them. Also shown for comparison is the PDF model based on Luhar and Sawford (1996) and a conservative empirically based equation derived using convective scaling arguments from Briggs (1985).

The most accurate approach of all of the models considered is the LPM model, which has been extensively tested against both laboratory and field data and described in many papers in the literature (see for example Franzese *et al*., 1999). For our purposes, we will take the results from this model as the correct result in order to compare the results from the alternative model options. It is also interesting to compare the results from the LPM to those of the PDF model and the CBL scaling model. The comparison shows (as expected) that both of these models are conservative, as both approaches neglect the time- and height-varying nature of the meteorology within the averaging period (1 hour), as well as along-wind diffusion effects.

The comparison of results for the various model options show that the predictions at a resolution of 750 m underestimate the maximum glcs, with the CGF predictions being higher than the EGM due to the inclusion of counter-gradient fluxes important in the convective boundary layer. At the 250 m resolution, both the EGM and CGF results are now higher than for the lower resolution. Results from both the EGM and CGF approaches are within about 20% of the LPM results, with CGF overestimating and EGM underestimating the LPM results for hours 9 and 10. Results for the rest of the day are similar for all three approaches. The predictions of all model options and resolutions are similar at the grid point 3 km downwind of the source.

6 Acknowledgments

Some of the methodologies and parameterisations used in TAPM have also been used in the Lagrangian Atmospheric Dispersion Model (LADM) of Physick *et al.* (1994), and experience gained by working with other team members on developing and applying LADM has proved to be invaluable in the development of TAPM.

The encouragement and advice of Peter Manins and Bill Physick, particularly in the later stages of model development, and on drafts of this document, are appreciated. Helpful comments from many people in CSIRO Atmospheric Research and CSIRO Energy Technology on various aspects of this work, including the implementation of some of the model parameterisations, are gratefully acknowledged.

Thanks to CSIRO Wildlife and Ecology for provision of the vegetation and soil type datasets, to Brian Weymouth for providing Cape Grim meteorological data, and to the Cape Grim Baseline Air Pollution Station and Arthur Downey of the Australian Bureau of Meteorology.

7 References

Andren, A. (1990). 'Evaluation of a turbulence closure scheme suitable for air pollution applications', *J. Appl. Meteorol.*, **29**, 224-239.

Azzi, M., Johnson, G.M., and Cope M. (1992). 'An introduction to the generic reaction set photochemical smog mechanism', *Proceedings of the 11th International Clean Air and Environment Conference*, Brisbane, 1992, Clean Air Society of Australia & New Zealand.

Baines, P.G., and Murray, D. (1991). 'Modelling of the airflow over Cape Grim', *Baseline 91*, 20-24.

Bermejo R., and Staniforth A. (1992). 'The conversion of semi-Lagrangian schemes to quasi-monotone schemes', *Mon. Wea. Rev.* **120**, 2622-2632.

Briggs G.A. (1975). 'Plume Rise Predictions. In *Lectures on Air Pollution and Environmental Impact Analysis*', Ed. D.A. Haugen, AMS, Boston, MA, pp. 59-111.

Briggs, G.A. (1985). 'Analytic parameterisations of diffusion : the convective boundary layer', *J. Clim. & Appl. Meteorol.*, **24**, 1167-1186.

Davies, H. (1976). 'A lateral boundary formulation for multi-level prediction models', *Q. J. R. Meteorol. Soc*. **102**, 405-418.

Deardorff, J.W. (1966). 'The counter-gradient heat flux in the lower atmosphere and in the laboratory', *J. Atmos. Sci.*, **23**, 503-506.

Derbyshire, S.H. (1990). 'Nieuwstadt's stable boundary layer revisited', *Q. J. R. Meteorol. Soc*. **116**, 127-158.

Dilley, A.C., and O'Brien, D.M. (1999). 'Estimating downward clear-sky long-wave irradiance at the surface from screen temperature and precipitable water', *Submitted to Q. J. R. Meteorol. Soc.*

Duynkerke, P.G. (1988). 'Application of the E-ε turbulence closure model to the neutral and stable atmospheric boundary layer', *J. Atmos. Sci.*, **45**, 865-880.

Duynkerke, P.G., and Driedonks, A.G.M. (1987). 'A model for the turbulent structure of the stratocumulus-topped atmospheric boundary layer', *J. Atmos. Sci.*, **44**, 43-64.

Dyer, A.J., and Hicks, B.B. (1970). 'Flux-gradient relationships in the constant flux layer', *Quart. J. Roy. Meteorol. Soc.*, **96**, 715-721.

Enger, L. (1986). 'A higher order closure model applied to dispersion in a convective pbl', *Atmos. Environ.*, **20**, 879-894.

Franzese, P., Luhar, A.K., and Borgas, M.S. (1999). 'An efficient Lagrangian stochastic model of vertical dispersion in the convective boundary layer.' *Atmos. Environ*., **33**, 2337-2345.

Garratt, J.R. (1992). 'The atmospheric boundary layer', Cambridge atmospheric and space science series, Cambridge University Press, Cambridge, 316 pp.

Gibson, M.M., and Launder, B.E. (1978). 'Ground effects on pressure fluctuations in the atmospheric boundary layer', *J. Fluid Mech.*, **86**, 491-511.

Glendening, J.W., Businger, J.A., and Farber, R.J. (1984). 'Improving Plume Rise Prediction Accuracy for Stable Atmospheres with Complex Vertical Structure', *J. Air Pollut. Control Ass.*, **34**, pp. 1128-1133.

Harley R.A., Russell A.G., McRae G.J., Cass G.R. & Seinfeld J.H. (1993). 'Photochemical modelling of the southern California air quality study', *Environ. Sci. Technol.*, **27**, 378-388.

Hurley, P.J. (1994). 'PARTPUFF - A Lagrangian particle/puff approach for plume dispersion modelling applications', *J. Appl. Meteorol.*, **33**, 285-294.

Hurley P.J., and Manins P.C. (1995). 'Plume rise and enhanced dispersion in LADM'. CSIRO Division of Atmospheric Research, ECRU Technical Note No. 4. 4 pp.

Johnson G.M. (1984). 'A simple model for predicting the ozone concentration of ambient air', *Proceedings of the 8th International Clean Air and Environment Conference*, New Zealand, 1984, Clean Air Society of Australia & New Zealand.

Katzfey, J.J., and Ryan, B.F. (1997). 'Modification of the thermodynamic structure of the lower Troposphere by the evaporation of precipitation: A GEWEX cloud system study', *Mon. Wea. Rev.*, **125**, 1431-1446.

Kowalczyk, E.A., Garratt, J.R., and Krummel, P.B. (1991). 'A soil-canopy scheme for use in a numerical model of the atmosphere - 1D stand alone model', CSIRO Division of Atmospheric Research Technical Report No. 23. 56 pp.

Luhar, A.K., Hibberd, M.F., and Hurley, P.J. (1996). 'Comparison of Closure Schemes used to Specify the Velocity PDF in Lagrangian Stochastic Dispersion Models for Convective Conditions.' *Atmos. Environ.*, **30**, 1407-1418.

Luhar, A.K., and Sawford, B.L. (1996) 'An examination of existing shoreline fumigation models and formulation of an improved model.' *Atmos. Environ.*, **30**, 609-620.

Mahrer, Y., and Pielke, R.A. (1977). 'A numerical study of the airflow over irregular terrain', *Beitr. Phys. Atmosph*., **50**, 98-113.

Manins, P., Ayers, G., Bohm, M., Raupach, M., Williams, D., and Carras, J. (1996). 'Hunter Valley Dry Deposition Study', Final report to Pacific Power, CSIRO Atmospheric Research.

McGregor J. (1993). 'Economical determination of departure points for semi-Lagrangian Models', *Mon. Wea. Rev.* **121**, 221-230.

McNider, R.T., and Pielke, R.A. (1981). 'Diurnal boundary-layer development over sloping terrain', *J. Atmos. Sci*., **38**, 2198-2212.

Mellor, G.L., and Yamada T. (1982) 'Development of a turbulence closure model for geophysical fluid problems', *Rev. Geophys. Space Phys*., **20**, 851-875.

Physick W.L. (1994). 'Calculation of dry deposition in LADM', CSIRO Division of Atmospheric Research ECRU Technical Note No. 1.

Physick, W.L., Noonan, J.A., McGregor, J.L., Hurley, P.J., Abbs, D.J., and Manins, P.C. (1994). 'LADM: A Lagrangian Atmospheric Dispersion Model', CSIRO Division of Atmospheric Research Technical Report No. 24. 137 pp.

Pielke R.A. (1984). 'Mesoscale Meteorological modelling', Academic Press, Orlando, 612 pp.

Puri, K., Dietachmayer, G.S., Mills, G.A., Davidson, N.E., Bowen, R.A., and Logan L.W. (1998). 'The BMRC Limited Area Prediction System, LAPS', *Aust. Met. Mag*., **47**, 203-223.

Rodi, W. (1985). 'Calculation of stably stratified shear-layer flows with a buoyancy-extended k-ε turbulence model', in J.C.R. Hunt (ed.), *Turbulence and diffusion in stable environments*, Clarendon Press, Oxford, 111-143.

Seinfeld, J.H., and Pandis, S.N. (1998). 'Atmospheric chemistry and physics from air pollution to climate change', Wiley, New York, 1326 pp.

Stephens, G.L. (1978). 'Radiation profiles in extended water clouds II : Parameterisation schemes'. *J. Atmos. Sci.*, **35**, 2123-2132.

Venkatram A., Karamchandani P., Prasad P., Sloane C., Saxena P., and Goldstein R. (1997). 'The development of a model to examine source-receptor relationships for visibility on the Colorado Plateau', *Journal of the Air and Waste Management Association*, **47**, 286-301.

Wesley M.L. (1989). 'Parameterisation of surface resistances to gaseous dry deposition in regional-scale numerical models', *Atmos. Environ.*, **23**, 1293-1304.

Willmott C.J. (1981). 'On the Validation of Models', *Phys. Geography*, **2**, 184-194.

CSIRO Atmospheric Research Technical Papers

This series was formerly issued as *Division of Atmospheric Research Technical Paper* (nos. 1-19); *CSIRO Division of Atmospheric Research Technical Paper* (nos. 20-37).

No. 1 Galbally, I.E.; Roy, C.R.; O'Brien, R.S.; Ridley, B.A.; Hastie, D.R.; Evans, W.J.F.; McElroy, C.T.; Kerr, J.B.; Hyson, P.; Knight, W.; Laby, J.E. Measurements of trace composition of the Austral stratosphere: chemical and meteorological data. 1983. 31 p.

No. 2 Enting, I.G. Error analysis for parameter estimates from constrained inversion. 1983. 18 p.

No. 3 Enting, I.G.; Pearman, G.I. Refinements to a one-dimensional carbon cycle model. 1983. 35 p.

No. 4 Francey, R.J.; Barbetti, M.; Bird, T.; Beardsmore, D.; Coupland, W.; Dolezal, J.E.; Farquhar, G.D.; Flynn, R.G.; Fraser, P.J.; Gifford, R.M.; Goodman, H.S.; Kunda, B.; McPhail, S.; Nanson, G.; Pearman, G.I.; Richards, N.G.; Sharkey, T.D.; Temple, R.B.; Weir, B. Isotopes in tree rings. 1984. 86 p.

No. 5 Enting, I.G. Techniques for determining surface sources from surface observations of atmospheric constituents. 1984. 30 p.

No. 6 Beardsmore, D.J.; Pearman, G.I.; O'Brien, R.C. The CSIRO (Australia) Atmospheric Carbon Dioxide Monitoring Program: surface data. 1984. 115 p.

No. 7 Scott, J.C. High speed magnetic tape interface for a microcomputer. 1984. 17 p.

No. 8 Galbally, I.E.; Roy, C.R.; Elsworth, C.M.; Rabich, H.A.H. The measurement of nitrogen oxide (NO, NO2) exchange over plant/soil surfaces. 1985. 23 p.

No. 9 Enting, I.G. A strategy for calibrating atmospheric transport models. 1985. 25 p.

No. 10 O'Brien, D.M. TOVPIX: software for extraction and calibration of TOVS data from the high resolution picture transmission from TIROS-N satellites. 1985. 41 p.

No. 11 Enting, I.G.; Mansbridge, J.V. Description of a two-dimensional atmospheric transport model. 1986. 22 p.

No. 12 Everett, J.R.; O'Brien, D.M.; Davis, T.J. A report on experiments to measure average fibre diameters by optical fourier analysis. 1986. 22 p.

No. 13 Enting, I.G. A signal processing approach to analysing background atmospheric constituent data. 1986. 21 p.

No. 14 Enting, I.G.; Mansbridge, J.V. Preliminary studies with a two- dimensional model using transport fields derived from a GCM. 1987. 47 p.

No. 15 O'Brien, D.M.; Mitchell, R.M. Technical assessment of the joint CSIRO/Bureau of Meteorology proposal for a geostationary imager/ sounder over the Australian region. 1987. 53 p.

No. 16 Galbally, I.E.; Manins, P.C.; Ripari, L.; Bateup, R. A numerical model of the late (ascending) stage of a nuclear fireball. 1987. 89 p.

No. 17 Durre, A.M.; Beer, T. Wind information prediction study: Annaburroo meteorological data analysis. 1989. 30 p. + diskette.

No. 18 Mansbridge, J.V.; Enting, I.G. Sensitivity studies in a two- dimensional atmospheric transport model. 1989. 33 p.

No. 19 O'Brien, D.M.; Mitchell, R.M. Zones of feasibility for retrieval of surface pressure from observations of absorption in the A band of oxygen. 1989. 12 p.

No. 20 Evans, J.L. Envisaged impacts of enhanced greenhouse warming on tropical cyclones in the Australian region. 1990. 31 p. [Out of print]

No. 21 Whetton, P.H.; Pittock, A.B. Australian region intercomparison of the results of some general circulation models used in enhanced greenhouse experiments. 1991. 73 p. [Out of print]

No. 22 Enting, I.G. Calculating future atmospheric CO2 concentrations. 1991. 32 p.

No. 23 Kowalczyk, E.A.; Garratt, J.R.; Krummel, P.B. A soil-canopy scheme for use in a numerical model of the atmosphere — 1D stand- alone model. 1992. 56 p.

No. 24 Physick, W.L.; Noonan, J.A.; McGregor, J.L.; Hurley, P.J.; Abbs, D.J.; Manins, P.C. LADM: A Lagrangian Atmospheric Dispersion Model. 1994. 137 p.

No. 25 Enting, I.G. Constraining the atmospheric carbon budget: a preliminary assessment. 1992. 28 p.

No. 26 McGregor, J.L.; Gordon, H.B.; Watterson, I.G.; Dix, M.R.; Rotstayn, L.D. The CSIRO 9-level atmospheric general circulation model. 1993. 89 p.

No. 27 Enting, I.G.; Lassey, K.R. Projections of future CO2. with appendix by R.A. Houghton. 1993. 42 p.

No. 28 [Not published]

No. 29 Enting, I.G.; Trudinger, C.M.; Francey, R.J.; Granek, H. Synthesis inversion of atmospheric CO2 using the GISS tracer transport model. 1993. 44 p.

No. 30 O'Brien, D.M. Radiation fluxes and cloud amounts predicted by the CSIRO nine level GCM and observed by ERBE and ISCCP. 1993. 37 p.

No. 31 Enting, I.G.; Wigley, T.M.L.; Heimann, M. Future emissions and concentrations of carbon dioxide: key ocean/atmosphere/land analyses. 1994. 120 p.

No. 32 Kowalczyk, E.A.; Garratt, J.R.; Krummel, P.B. Implementation of a soil-canopy scheme into the CSIRO GCM — regional aspects of the model response. 1994. 59 p.

No. 33 Prata, A.J. Validation data for land surface temperature determination from satellites. 1994. 40 p.

No. 34 Dilley, A.C.; Elsum, C.C. Improved AVHRR data navigation using automated land feature recognition to correct a satellite orbital model. 1994. 22 p.

No. 35 Hill, R.H.; Long, A.B. The CSIRO dual-frequency microwave radiometer. 1995. 16 p.

No. 36 Rayner, P.J.; Law, R.M. A comparison of modelled responses to prescribed CO2 sources. 1995. 84 p.

No. 37 Hennessy, K.J. CSIRO Climate change output. 1998. 23 p.

No. 38 Enting, I. G. Attribution of greenhouse gas emissions, concentrations and radiative forcing. 1998. 29 p.

No. 39 O'Brien, D.M.; Tregoning, P. Geographical distributions of occultations of GPS satellites viewed from a low earth orbiting satellite. 1998. 23 p.

No. 40 Enting, I. G. Characterising the temporal variability of the global carbon cycle. 1999. 23 p.

No. 42 Mitchell, R. M. Calibration Status of the NOAA AVHRR Solar Reflectance Channels: CalWatch Revision 1. 1999. 20 p.

Address and Contact Details: CSIRO Atmospheric Research
Private Bag No.1 Aspendale Victoria 3195 Australia
Ph: (+61 3) 9239 4400; fax: (+61 3) 9239 4444
e-mail: chief@dar.csiro.au